(A New Proposal to Jefferson Lab PAC25)

# High resolution study of the 1540 exotic state


J. P. Chen, E. Chudakov, C. DeJager, P. Degtyarenko, R. Feuerbach, M. Jones,
J. Gomez, O. Hansen, D. W. Higinbotham, J. LeRose, W. Melnitchouk,
R. Michaels, S. Nanda, B. Reitz, A. Saha, B. Wojtsekhowski (spokesperson)
*Thomas Jefferson National Accelerator Facility, Newport News, VA 23606*

J. Arrington, K. Hafidi, R. Holt, P. E. Reimer(co-spokesperson),
D. Potterveld, X. Zheng
*Argonne National Laboratory, Argonne, IL 60439*

D. Nikolenko, I. Rachek
*Budker Institute, Novosibirsk, Russia*

G. B. Franklin, B. Quinn, R. Schumacher, C. Meyer
*Carnegie Mellon University, Pittsburgh, PA 15213*

L. Pentchev
*College of William and Mary, Williamsburg, VA 23185*

P. Markowitz
*Florida International University, Miami, FL 33199*

F. Cusanno, F. Garibaldi, S. Frullani, G. M. Urciuoli, M. Iodice
*INFN, Rome, Italy*

R. De Leo, L. La Gamba
*INFN, Bari, Italy*

A. Asratyan, G. Davidenko, A. Dolgolenko, G. Dzyubenko, V. Evdokimov, V. Goryachev,
M. Kubantsev, I. Larin, V. Matveev, A. Sitnikov, V. Verebryusov, V. Vishnyakov
*Institute of Experimental and Theoretical Physics, Moscow, Russia*

O. Gayou
*Massachusetts Institute of Technology, Cambridge, MA 02139*

Ya. Azimov
*PNPI of Russian Academy of Science, Gatchina, Russia*

M. Polyakov
*Inst. de Physique au Sart-Tilman, B5a Univ. de Liege B4000 Liege 1, Belgium*
*Institute for Theoretical Physics II Ruhr University, 4470 Bochum, Germany*
*Petersburg Nuclear Physics Institute Gatchina, St. Petersburg, 188350 Russia*

V. Kubarovsky*, P. Stoler
*Rensselaer Polytechnic Institute, Troy, NY 12180-3590*

R. Gilman, K. McCormick
*Rutgers, The State University of New Jersey, Piscataway, NJ 08854*

P. Souder, R. Holmes, B. Hachemi .
*Syracuse University, Suracuse, NY 13244*

E. Piasetzky
*Tel Aviv University, Israel*

W. Briscoe, R. Arndt, I. Strakovsky, R. Workman
*Center for Nuclear Studies, Department of Physics*
*The George Washington University, Washington DC 20052*

W. Korsch
*The University of Kentucky, Lexington, KY 40506*

J. Annand, D. Ireland, J. Kellie, K. Livingston, G. Rosner
*University of Glasgow, Glasgow, Scotland*

A.M. Nathan
*University of Illinois, Champaign-Urbana, IL 61801*

K. Kumar, K. Paschke, L. Kaufman
*University of Massachusets, Amherst, MA*

J. Calarco, W. Hersman
*University of New Hampshire, Durham, NH 03824*

G. Cates, D. Day, A. Deur, R. Lindgren, N. Liyanage, V. Nelyubin†,
B. E. Norum, J. Singh, R. Snyder, W. A. Tobias, K. Wang
*University of Virginia, Charlottesville, VA 22901*

K. Egiyan, S. Mayilyan, V. Mamyan, A. Shahinyan
*Yerevan Physics Institute, Yerevan, Armenia*

and
**The Hall A Collaboration**

† on leave from PNPI of Russian Academy of Sciences, Gatchina, Russia
* also TJNAF, Newport News, VA 23606

December 2, 2003

**Abstract**

An experiment is proposed which will measure the parameters of an exotic $S = +1$ baryonic state recently observed in the reaction $\gamma n \to K^- \Theta^+ \to K^- K^+ n$. Three closely connected studies are proposed here:

(1) The investigation of the reaction D$(e, K^- n K^+)$X, which will measure the resonance mass and width with a resolution (FWHM) of 2.9 MeV and an angular distribution of the decay products, which may allow determination of the $\Theta^+$ spin.

(2) The investigation of the reaction D$(e, e' K^- p_{soft})$X , which will measure the resonance mass with an accuracy (systematic) of 1.3 MeV and width with a resolution (FWHM) of 3.4 MeV; and estimate of the photon linear polarization asymmetry, which may provide a key to $\Theta^+$ parity. Both measurements will find the production cross section.

(3) The investigation of the reaction H$(e, e' K^-)$X [and H$(e, e' K^+)$X], which will search for the $\Theta^+$ state partners, namely a $\Theta^{++}$ in the mass range 1450-1620 MeV and a $\Sigma^{\circ}_{\overline{10}}$ in the mass range 1560-1860 MeV.

The experiment utilizes a 4.5(6.0) GeV electron beam in Hall A, HRS spectrometers with the septum magnets, the BigBite spectrometer, and a large neutron detector. This equipment exists or is under construction for recently approved experiments. With 1116 hours of beam-time for all three measurements, data will be obtained on the resonance width, mass, and quantum numbers. Such measurements will dramatically increase our experimental confidence in the parameters of the exotic state and its nature.

# 1 Introduction

A new baryon resonance ($\Theta^+$) has been observed in $K^+n$ and $K^o_s p$ decays by several independent experiments [3, 4, 5, 6, 7, 8, 9]. Because of its positive strangeness and baryon number, the $\Theta^+$ is explicitly exotic, and its minimal quark content is $uudd\bar{s}$. Such a state was predicted as a member of an antidecuplet of the flavor group $SU(3)_F$ [1]. This unitary identification assumes zero isospin of the $\Theta^+$, and continues to be favored [10, 11, 12]. However, other identifications with higher isospin have also been suggested in the literature [13, 14]. These suggestions imply the existence of related states such as the $\Theta^{++}$. An alternative idea on the origin of the small width of the $\Theta^+$ was suggested in [15].

The mass of the $\Theta^+$ was predicted to be 1530 MeV [1]. Several of the present experiments give the nearby value of 1540 MeV, with a range of 1526-1555 MeV (see Tab. 1).

| Aprroach/ Collaboration | Beam/Target | Channel | Mass (MeV) | Width (MeV) | Ref. |
|---|---|---|---|---|---|
| Theoretical Predictions | | | | | |
| Chiral soluton | | | 1530 | <15 | [1] |
| Experimental Observations | | | | | |
| LEPS | $\gamma^{12}C$ | $nK^+$ | 1540±10 | <25 | [3] |
| DIANA | $K^+Xe$ | $pK^\circ_s$ | 1539±2 | <9 | [4] |
| CLAS/$\gamma n$ | $\gamma D$ | $nK^+$ | 1542±5 | <21 | [5] |
| CLAS/$\gamma p$ | $\gamma H$ | $nK^+$ | 1555±16 | <26 | [6] |
| ELSA | $\gamma H$ | $nK^+$ | 1540±4±2 | <25 | [7] |
| ITEP/$\nu$ | $\nu H, D, Ne/H$ | $pK^\circ_s$ | 1533±5 | <20 | [8] |
| HERMES | $eD$ | $pK^\circ_s$ | 1526±2±2 | <18 | [9] |
| Limits based on *Non*-Observations | | | | | |
| USC | $K^+d$ | | 1543 | <6 | [16] |
| GWU | $K^+n$ | | 1540−1550 | ≤1 | [17] |
| Jülich | $K^+n$ | | 1545 | <5 | [18] |

Table 1: Theoretical predictions, experimental observations and limits based on non-observation for the production of the $\Theta^+$.

The spin of the $\Theta^+$ is unknown, though there is weak evidence that $J = 1/2$ is preferred, as was predicted [1]. Many models predicted a positive parity, but lattice gauge calculations [2] and constituent quark model predicted a negative one. The parity puzzle has sparked lively discussion in the literature, since $uudd\bar{s}$ positive parity state requires at least one unit of orbital angular momentum in the quark configuration.

The most intriguing property today is the width of the $\Theta^+$. The original theoretical prediction had $\Gamma_{\Theta^+} < 15$ MeV [1]. Existing experiments cannot resolve $\Gamma_{\Theta^+}$, however they place upper limits based upon the experimental resolution. Most experimental publications give an upper boundary of 20 MeV, larger than expected by theory. The Xenon bubble chamber data, corresponding in essence to the charge exchange $K^+n \to K^0p$, provide a tighter limit of 9 MeV [4]. An indirect data treatment [16], using the published $K^+d$ total cross section data, leads to a stronger limitation $\Gamma_{\Theta^+} < 6$ MeV. The partial-wave analysis of available $KN$ (elastic and charge exchange) scattering data appear to exclude even widths above 1 MeV [17]. If the width is indeed so small, it is natural to expect that other members of the same multiplet should have comparable widths. Such an expectation is supported by recent evidence for another exotic state $\Xi^{--}$ also having a narrow width [19]. A width on the level of few MeV will indicate that the $\Theta^+$ has very different structure than known baryons.

Our primary goal will be a measurement of the width of the $\Theta^+$. It will be achieved by using basic JLab Hall A spectrometers which are capable of providing sub-MeV energy resolution in electro/photo production of the resonance, small angle, high momentum particle detection and excellent PID for few GeV kaons, and the "third" arms of Hall A which are under development for the already approved experiments E01-014 [20] and E02-013 [21], namely the BigBite spectrometer and the large neutron detector. The value of the $\Theta^+$ mass will also be measured. The angular distribution of the decay products will be measured and may allow for the determination of the resonance spin. The photon linear polarization asymmetry will also be measured, which may provide a key to the $\Theta^+$ parity.

There are two other members of the possible antidecuplet which might also be readily observed using the same detector system, namely the $\Sigma^-_{\overline{10}}$ and the $\Sigma^\circ_{\overline{10}}$. A search for the $\Theta^{++}$ member of the proposed isotensor multiplet [13] will also be performed. A search, similar to that of the $\Theta^+$, has found no evidence for the $\Theta^{++}$ in existing $K^+p$ scattering data [17], where the authors did an evaluation for the mass range of 1520 to 1560 MeV and for the width range of 0.1 to 10 MeV. The production process $p(e, e'K^-)Z$ was discussed in detail by [22]. The Hall A two septum setup has very high sensitivity in the search for both the $\Sigma^\circ_{\overline{10}}$ and the $\Theta^{++}$.

We, therefore, propose a search and a study of the exotic baryon in electromagnetic reactions from the neutron and proton. The proposal is organized as follows. In section 1 we present the physics motivation and the goals of the proposed experiment. Section 2 introduces the kinematics of the proposed measurements. In section 3 we describe essential features of both the standard and the specialized equipment. Section 4 summarizes experimental information for inclusive photo-production of the negative kaons in the diffractive regime, which allow us to make an estimate of the non-resonant and accidental background contributions to the expected data and calculation of the single rates in detectors. Section 5 presents the details of proposed measurements, the calculations of the mass resolution, event rates, trigger logic, and event analysis. Expected results and a beam time request are shown in section 6. Finally the proposal is summarized in section 7.

## 2 Kinematics

The diagram of the reaction is shown in Fig. 1. The quasi-real photons are produced by electron scattering. A pair of kaons is produced through the diffractive mechanism with $t$-channel dominance. The virtual kaon interaction with a neutron results in the $\Theta^+$. The $\Theta^+$ state decays into the $K^+$ and the neutron. The narrow width of the $\Theta^+$ means that its decay is most likely to happen at a large distance from the target nuclei. The reaction is characterized by small angle between negative kaon and photon momenta or low $t$-dominance. The dominant exchange particles are the pseudo-scalar $K^+$ and the much more massive vector $K^{+*}$. As illustrated in Figs. 2 and 3 this experiment will study the production of the

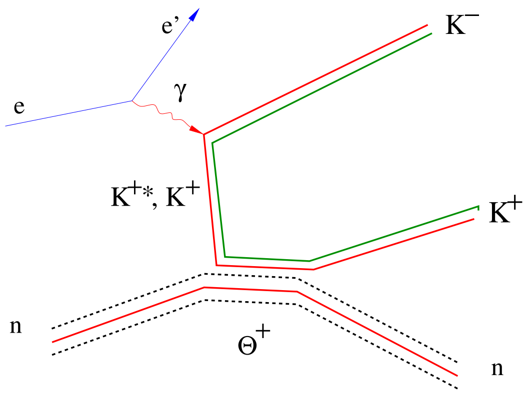


Figure 1: The diagram of the $\Theta^+$ production process.

$\Theta^+$ from a deuterium target. The high-energy forward-going negative kaon will be detected in the Left High Resolution Spectrometer (HRS-left). In **the first part of the experiment (M1)** the scattered electron will remain undetected. Both decay products of the $\Theta^+$ will be detected and provide full information about the $\Theta^+$ four-momentum. The positive kaon will be detected in BigBite and the neutron in the large neutron detector. In **the second part of experiment (M2)**, the secondary electron will be detected in HRS-right. The soft proton will be detected in BigBite to complete information about the missing momentum and allow accurate reconstruction of the $\Theta^+$ momentum and mass. These detectors are built or under construction for approved experiments E01-014 [20] and E02-013 [21]. In **the third part of the experiment (M3)** the high momentum kaon (positive in search for the $\Sigma^{\circ}_{\overline{10}}$ and negative in search for the $\Theta^{++}$) will be detected in HRS-left, and the scattered electron will be detected in HRS-right. The order in which the measurements will be performed can differ from the introduction above because of schedule opportunities and equipment readiness.

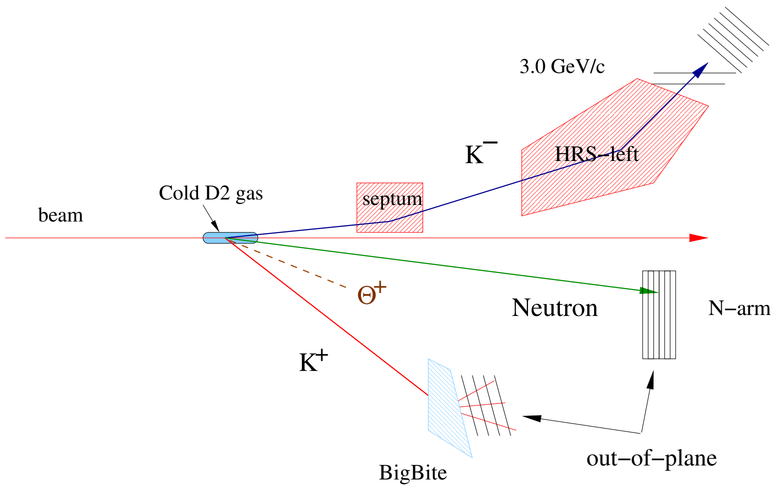


Figure 2: The experimental setup for the first part of the experiment.

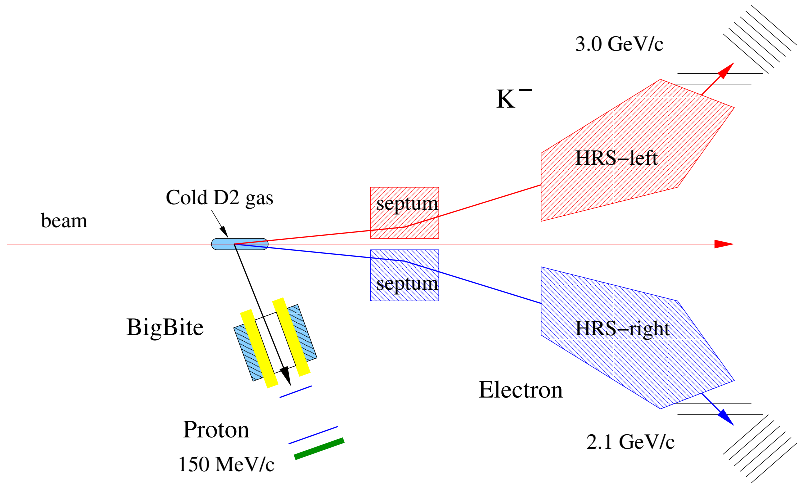


Figure 3: The experimental setup for the second and the third (M2 and M3) parts of the experiment. In the third part of the experiment BigBite will not be used.

## 2.1 The kinematics in M1

An electron beam with a current of 20 $\mu$A at an energy of 4.5 GeV will be used. The density of the gas target will be adjusted to obtain an electron-nucleon luminosity $\mathcal{L}_{eN(ucleon)}$ of $1 \cdot 10^{37}$ cm$^{-2}$s$^{-1}$. The negative kaon will be detected in the magnetic spectrometer HRS-left at a central angle of 6° with a septum magnet. The positive kaon will be detected in the BigBite spectrometer at horizontal/vertical angles 18°/-15°, and the neutron will be detected in the large neutron detector at horizontal/vertical angles 18°/+22° (see Fig. 2). HRS-left is selected for kaon detection because it is equipped with threshold Čerenkov counters for pion rejection at the trigger level [23] and the state-of-the art RICH detector for identifying the kaon [24]. The selected kaon momentum of 3 GeV/$c$ follows from improved kaon survival probability at high momentum and the upper limit of the kaon PID (2.84 GeV/$c$). The kaon momentum of 3 GeV/$c$ is also consistent with the photon energy and the angle of the spectrometer. The photon energy of 4 GeV leads to the choice of 4.5-5 GeV electron beam energy because with higher beam energy the Feynman variable $x_F$ become smaller and inclusive $K^-$ photo-production cross section is growing which leads to larger non-resonance background. Also, at lower beam energy the flux of equivalent photons is reduced.

The direction of the $\Theta^+$ particle is about 18°. The relatively small momentum of the produced $\Theta^+$ (of 1 GeV/$c$) and low energy yield in its decay to the $K^+n$ channel leads to a large angle between $K^+$ and neutron. The forward direction of the $\Theta^+$ leads to positioning the detectors in a place with high background rate. Especially if the detectors are located in the same plane as the negative kaon. So, we plan to put both detectors out-of-plane. The BigBite will be installed in the direction down by 15° and the neutron detector in the direction up by 22°. Such an arrangement has a relatively large angle between the beam line and detectors (25-30°) and also a large range of angles between the $\Theta^+$ momentum and decay products (due to the favorable aspect ratio of the acceptance in BigBite and the neutron detector) which is very important for determining the resonance spin.

## 2.2 The kinematics in M2

An electron beam with a current of 110 $\mu$A at an energy of 6 GeV will be used. The density of the gas target will be adjusted to obtain the $\mathcal{L}_{eN}$ of $1.1 \cdot 10^{38}$ cm$^{-2}$s$^{-1}$. As was suggested above, the negative kaon will be detected in the magnetic spectrometer HRS-left at a central angle 6° with a septum magnet. The scattered electron will be detected in the magnetic spectrometer HRS-right at a central angle 6° with the second septum magnet. The soft proton will be detected in the BigBite spectrometer at a central angle of 70°.

In this measurement the resonance will remain undetected, but observed in the missing mass spectrum in the reaction D$(e, e'K^- p_{soft})$X . It requires detection of the electron, the negative kaon, and the proton. To achieve sufficient counting rate in this approach we rely on the detection of a very soft proton. We propose using a cold gas target. Because of large length of the cell, the required luminosity can be obtained with gas density which is only of 2-3% of the liquid deuterium density. The threshold momentum for the proton can be as low as 150 MeV/$c$. We find that the optimum direction for the soft proton, in which BigBite can be used together with two HRSs and septum magnets, is about 70°. We also note that for such slow protons the time-of-flight can provide sufficient momentum resolution for this experiment. The combination of the wire chamber and a segmented ToF plane could be used instead of full BigBite spectrometer. However, because the background study was done only for BigBite we will consider it as the primary option for the second measurement in this proposal.

The central momentum of the kaon spectrometer will correspond to the quasi-free production of the $\Theta^+$ from the neutron by a quasi-real photon with an energy of 4.0 GeV. The significantly larger electron beam energy as compared to first measurement leads to a larger energy of the final electron and larger momentum acceptance of the spectrometer. The scattered electron energy will be about 2.1 GeV, which corresponds to the range of missing masses of 1480 to 1620 MeV.

### 2.3 The kinematics in M3

An electron beam with a current of 100 $\mu$A at an energy of 6 GeV will be used. The density of the gas target will be adjusted to obtain the $\mathcal{L}_{eN}$ of $1 \cdot 10^{38}$ cm$^{-2}$s$^{-1}$. The measurement can be done with the standard Hall A cryogenic target, but with a significant loss of resolution due to multiple scattering in the target. The kaon will be detected in the magnetic spectrometer HRS-left at a central angle of 6° with a septum magnet. The scattered electron will be detected in the magnetic spectrometer HRS-right at a central angle of 6° with the second septum magnet. There will be one momentum setting in the search for the $\Theta^{++}$ and two settings (to cover a larger range of the missing mass) in the search for the $\Sigma^{\circ}_{\overline{10}}$. The polarity of HRS-left will be positive in the search for the $\Sigma^{\circ}_{\overline{10}}$ and negative in search for the $\Theta^{++}$. The instrumental resolution in missing mass in such a measurement (FWHM) will be $\approx$1.75 MeV.

# 3 Experimental Setup

The experiment will be performed in Hall A, where the spectrometers equipped with the septum magnets provide access to scattering angles of 6°. The Hall A spectrometers also have powerful particle ID. Kaon identification in HRS-left includes a time-of-flight system with a resolution of 150 ps and threshold Čerenkov counters. A Ring Imaging Čerenkov detector in HRS-left is being commissioned. For proton rejection in BigBite, a threshold Čerenkov counter with a water radiator will be constructed. For pion rejection, another threshold Čerenkov counter with the aerogel radiator will be constructed.

## 3.1 The CEBAF electron beam

The beam energy of 4.5 GeV will be used in the first part of this experiment. For the second (and third) part of the experiment a higher beam energy of 6.0 GeV should give a better signal-to-background ratio.

## 3.2 The cold gas deuterium target

The experiment will utilize the standard Hall A liquid hydrogen target system, but with a new target cell, shown in Fig. 4. It is a 50-cm long combined machined-soldered cell with 2 cm diameter and 25 $\mu$m wall thickness of Al (or 100 $\mu$m of Be). The cell will be filled with deuterium at 28 K and a pressure of about 2 atm. The density will be of 0.040 g/cm$^2$. The parameters will be adjusted for specific luminosity of each measurement. The large length of the target allows us to reduce the gas density and pressure, which is important for reducing soft proton scattering in the gas and the walls of the cell. Another important advantage of the long target is the suppression of the accidental events.

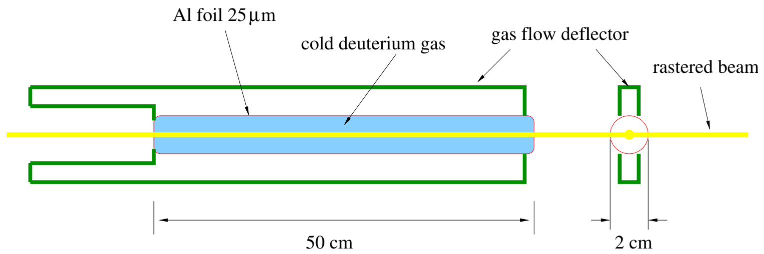


Figure 4: The concept of the long cold gas target.

## 3.3 The High Resolution Spectrometer-left

Basic parameters of the HRS-left are given in Tab. 2. The spectrometer has very good momentum and angular resolutions and moderate momentum and angular acceptances.

| item | value |
|---|---|
| central momentum range, $p_c$ [GeV/$c$] | 0.3-4.3 |
| momentum acceptance, $\Delta p/p_c$ [%] | $\pm$ 4.5 |
| momentum resolution, $\sigma_p/p$ | $1.1 \cdot 10^{-4}$ |
| minimum angle for the central trajectory | $6°$ with septum |
| solid angle for the point target [msr] | 6.2 |
| coverage for scattering angle | $3.1°$ |
| extended target acceptance, Y [cm] | $\pm$ 5 |
| $\theta_{disp}$ angular resolution (rms) [mr] | 1.5 |
| $\theta_{nondisp}$ angular resolution (rms) [mr] | 2.0 |
| target vertex Y resolution, $\sigma_Y$ [mm] | 1.5 |
| path from the target to the trigger [m] | 25.0 |
| detector area (front chamber), [cm x cm] | $200 \times 15$ |
| trigger segmentation | 16 |
| time resolution, $\sigma_{ToF}$ [ns ] | 0.15 |

Table 2: The parameters of the HRS spectrometer.

#### 3.3.1 The HRS-left particle identification

HRS-left has several means for particle identification, especially for selecting high energy kaons. The PID can be used for on-line rejection of electrons and pions as well as for off-line selection of a very clean kaon event sample. There are two threshold Čerenkov counters in HRS-left called A1 and A2 with indices of refraction of 1.015 and 1.055, respectively. The A1 is perfectly suitable for use in the trigger for rejection of the electrons and pions with kaon momentum up to 2.84 GeV/$c$. The effectiveness of these counters was shown during experiments E98-108 and in 2001 and 2002 (see Fig. 5). The detector package in HRS has two scintillator planes. Recently, the second plane in each HRS was replaced by a new one, for which the time resolution (sigma) is about 150 ps per paddle. This will allow us to realize identification of the beam bursts by using the electron arm and measuring the kaon ToF with 150 ps resolution for the flight path of 25 meters. For unique identification of the kaon, the hyper-nuclei collaboration (E94-107) constructed a Ring Imaging Čerenkov detector. It has a liquid freon radiator and is perfect for kaon identification in the few GeV momentum range. The on-line rejection of electrons will be done using the A1 aerogel Čerenkov counter and enhanced by a factor of 10 with the pion rejector–a two layer shower detector, installed in the HRS-left.

### 3.4 The High Resolution Spectrometer-right

The second HRS, also with the septum magnet in $6°$ configuration, will be used to detect the scattered electrons during the second part of experiment. This spectrometer also has a vacuum connection to the scattering chamber. For electron identification the HRS-right has a highly efficient gas Čerenkov counter and a preshower/shower lead-glass detector, which

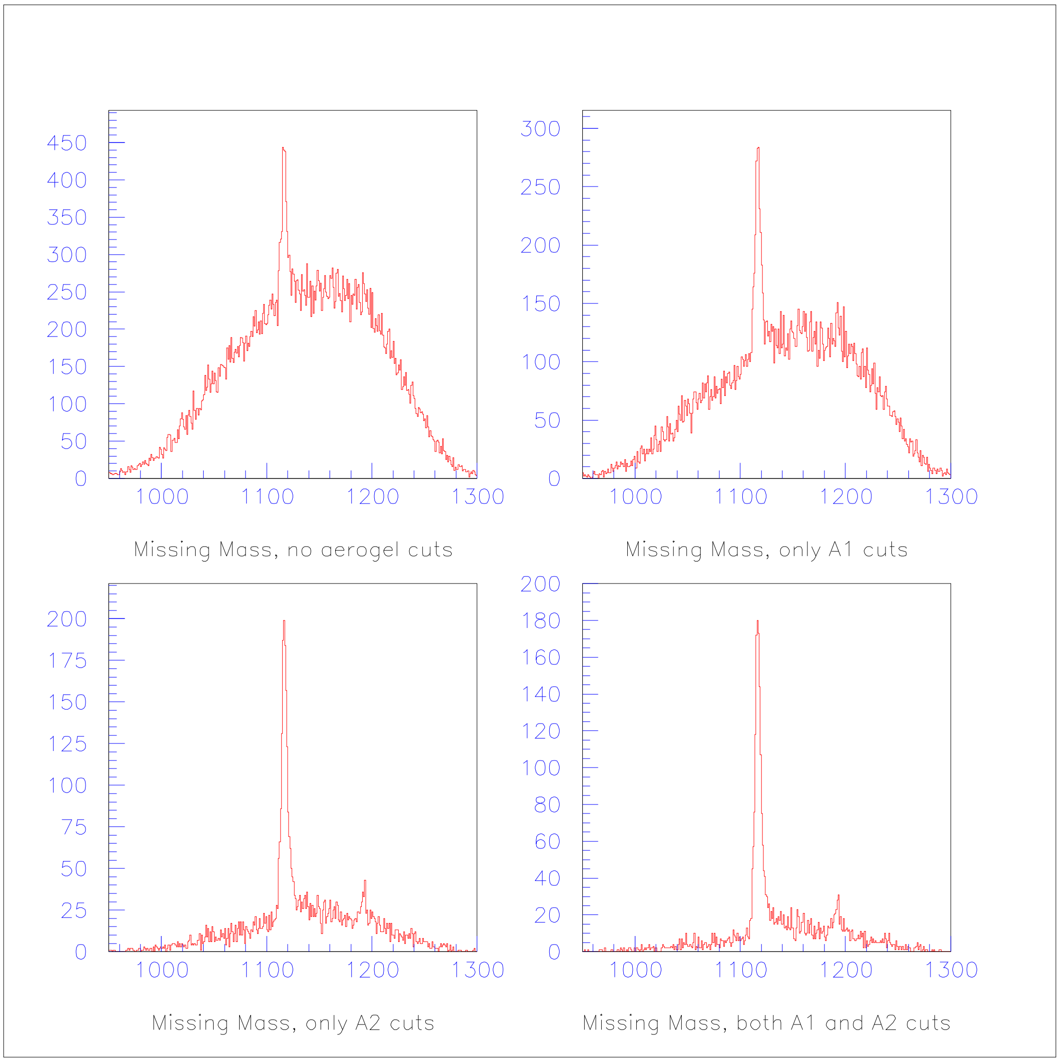


Figure 5: The missing mass spectra in $H(e, e'K^+)$ measurement with different PID cuts applied. The data are from experiment E98-108.

off-line have a combined pion rejection factor about $10^5$.

#### 3.4.1 Operation with the septum magnet

The first septum magnet was commissioned in July-August 2003 with HRS-right during E97-104 experiment. This experiment used a polarized $^3$He target, so in the first 180 cm after the target the electrons pass through the air causing significant scattering. Figure 6 shows the optic calibration data at a beam energy of 2.13 GeV. Raw analysis of the momentum spectra is shown in Fig. 7. The reconstruction of the target vertex is shown in Fig. 8. These data confirm that the HRS momentum and angular resolutions are about the same with and without the septum.

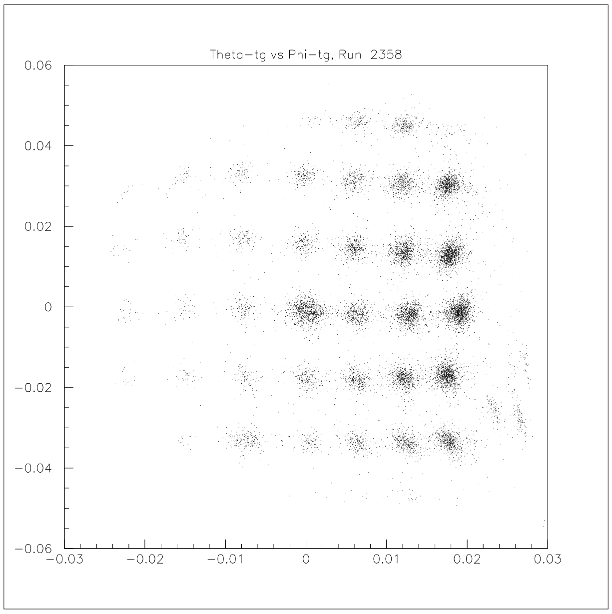


Figure 6: Sieve slit data for calibration of the optics at beam energy 2.13 GeV.

#### 3.4.2 The HRS-right particle identification

The PID detectors will be used for on-line rejection of the negative pions as well as for off-line analysis of the ToF. The HRS-right has a gas Čerenkov counter with a $CO_2$ radiator. An on-line pion rejection factor of 20 and off-line factor of 200-300 were obtained. The preshower/shower detector of HRS-right can also provide on-line pion rejection of a factor of 10 and off-line about 100-300. A new scintillator plane with time resolution of 150 ps will allow us to identify the beam bunch.

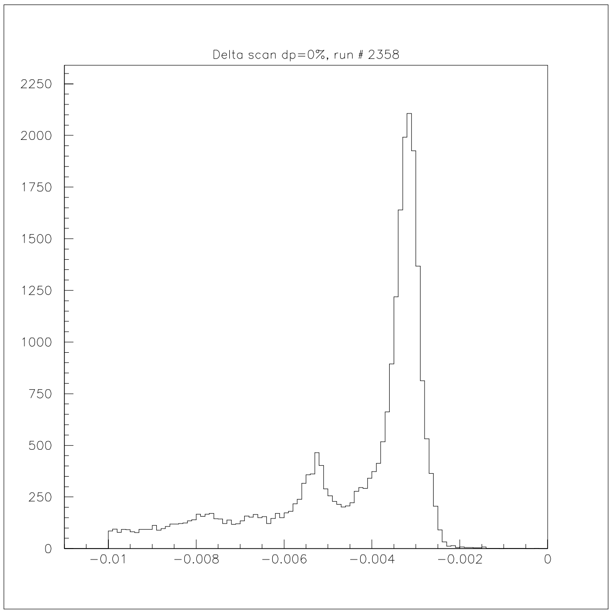


Figure 7: Momentum spectra for electron scattering from $^{12}$C with the septum at the beam energy 2.13 GeV.

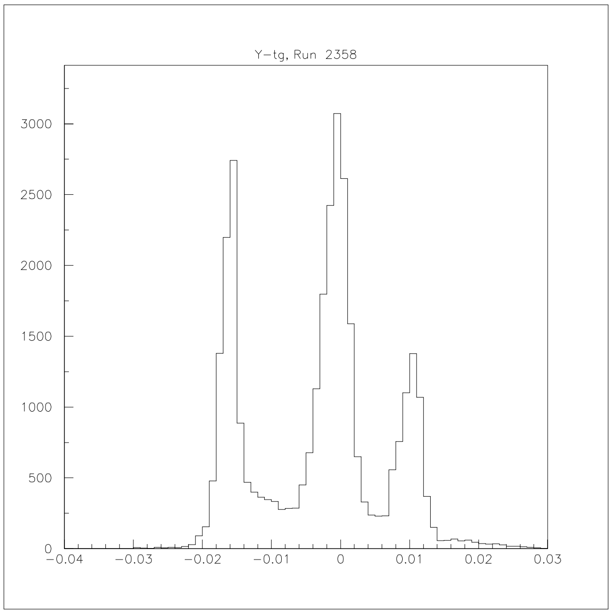


Figure 8: The on-line result for the target vertex reconstruction with the septum from three $^{12}$C foils located at -20, 0, and +10 cm along the beam direction.

### 3.5 The BigBite spectrometer

The BigBite spectrometer consists of a 20 ton dipole magnet and its detector system, which includes planes of drift chambers and trigger counters. The concept of such a spectrometer was developed and realized at NIKHEF [25]. The parameters observed for the detection of scattered electrons at NIKHEF are given in Tab. 3. For operation in Hall A at

| item | value |
|---|---|
| nominal momentum coverage (at H=9 kG) [MeV/$c$] | 200-900 |
| momentum resolution, $\sigma_p/p$ [%] | 0.5 |
| solid angle for the point target [msr] | 96 |
| $\theta$ angular resolution [mr] | 4.0 |
| target vertex resolution, $\sigma_Y$ [mm] | 5 |
| path from the target to the trigger [m] | 4.0 |
| detector area (front chamber), [cm x cm] | 140×35 |

Table 3: The generic parameters of the BigBite spectrometer [25].

higher luminosity, the original detector system is being modified. The new detector has a set of high resolution drift chambers. In both measurements (M1 and M2) the particle path from the target to the front wire chamber of BigBite will be in vacuum. The MC studies are done for the geometry of the present proposal for the detection of the $K^+$ and the soft proton. For 600 MeV/$c$ momentum $K$, the relative momentum resolution was found to be 0.6% and an angular resolution of 1-2 mr.

#### 3.5.1 The BigBite particle identification

BigBite is equipped with a two-layer scintillator trigger plane, which provide 0.20 ns ToF resolution and $\Delta E/E$ information. In the first part of the experiment two segmented Čerenkov counters with a water radiator (similar to that built for HKS [26]) and the aerogel radiator (n = 1.055, similar to the A2 detector in HRS-left) will be added to the BigBite detector package. Table 4 shows the calculated number of photo-electrons in the Čerenkov counters and the ToF difference between kaon and pion for different momenta. The water Čerenkov detector will be used for off-line positive identification of kaons at momenta above 600 MeV/$c$. Protons with momenta below 600 MeV/$c$ will be rejected with a factor of 100 using ToF. In the second part of the experiment, BigBite will be used to detect low momentum protons, which have time-of-flight in the range of 40-80 ns. The expected rate of the scintillator plane is of order 27 MHz, mostly pions. For 24 segments in the trigger plane this leads to about 1 MHz per paddle. The $\Delta E/E$ analysis should be sufficient for the suppression of the pion contamination by a factor of 20, after which pion contamination will be below 10%. Correlation of the velocity and momentum will be used for the suppression of accidental hits.

| momentum | average number of photo electrons | | | | | $\Delta$ ToF |
|---|---|---|---|---|---|---|
| [MeV/$c$] | $p$ in water | $K$ in water | $K$ in aerogel | $\pi$ in water | $\pi$ in aerogel | $K-\pi$ [ns] |
| 200 | 0 | 0 | 0 | 150 | 0 | 23.8 |
| 400 | 0 | 0 | 0 | 340 | 0 | 15.9 |
| 600 | 0 | 50 | 0 | 370 | 15 | 8.5 |
| 800 | 0 | 200 | 0 | 380 | 22 | 5.2 |
| 1000 | | 270 | 0 | 390 | 24 | 3.5 |

Table 4: The light collection (the average number of photo-electrons) in the Čerenkov counters and the difference between ToF for $K$ and $\pi$ in BigBite.

#### 3.5.2 Momentum - Time-of-Flight and vertex correlations

For protons with momenta as low as 150 MeV/$c$, the ToF information provides quite accurate momentum determination. This information, used in combination with coordinates in the front drift chamber, allow us to improve angular resolution in the dispersive direction. Correlation between ToF and momentum measured via deflection also provide the means for rejection of the accidental proton hits. In the present experiment two particles will be detected in the HRSs and provide determination of the event vertex in the target with an accuracy of 1 cm. This vertex position allows dramatic improvement in the angular resolution in the horizontal plane, which is quite important for the accurate determination of the missing mass.

### 3.6 The neutron detector

The large neutron detector is under construction for the GEN E02-103 experiment [21]. It consists of 244 neutron bars and 184 veto paddles. They are arranged in seven(six) layers with the iron converters and two veto planes. Figure 9 shows the schematic view of the detector cross section. The detector efficiency is about 20-30%, which takes into account a significant loss of neutrons from interactions in the front shielding and interactions which fire the veto counters. Each neutron bar is viewed by two PMTs, so the ToF resolution (rms) is approximately 0.3 ns. Because the neutron energy in the proposed experiment is much less than in GEN the trigger threshold will be reduced from 50 MeV to 20 MeV. We also plan to reduce the front shielding from 2 inch to 1 inch of Pb and the thickness of the steel plates (neutron converters), which also hold the plastic bars, from 1 inch to 0.5 inch. The detector efficiency as calculated with a GEANT4-based code is shown in Fig. 10 for different threshold levels.

The trigger scheme of the neutron arm is based on summing the signals from all counters of four vertical layers (total 32 bars) as shown in Fig. 9. The PMT signals in each two layers are summed together (denoted as SS1-15) and then used for the overlapping sums (denoted as S1-14). The output signals from S1-14 units will be discriminated and form the neutron arm trigger. The expected rate of the neutron arm trigger is about 1.9 MHz for a threshold of 20 MeVee. The rate of individual PMTs is expected to be about 60 kHz with a threshold of 5 MeVee.

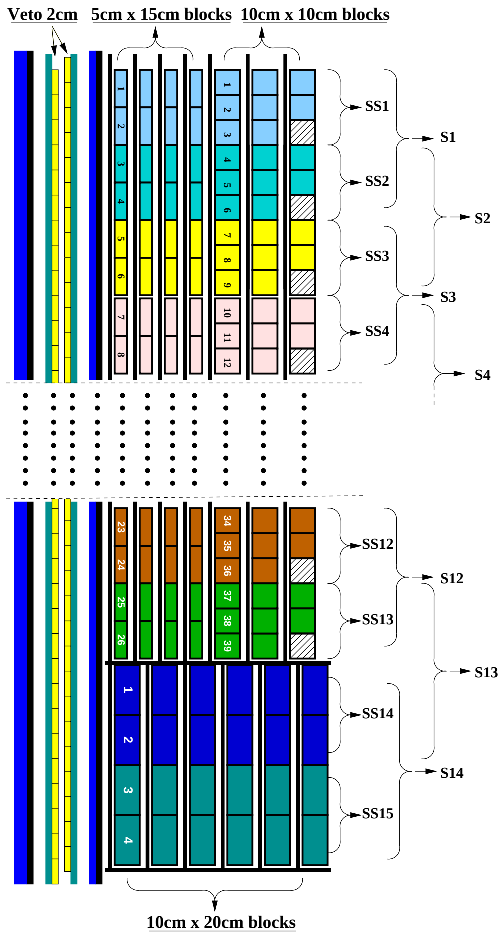


Figure 9: The scheme of the neutron detector and the groups of the counters whose signals will be summed for use in the trigger.

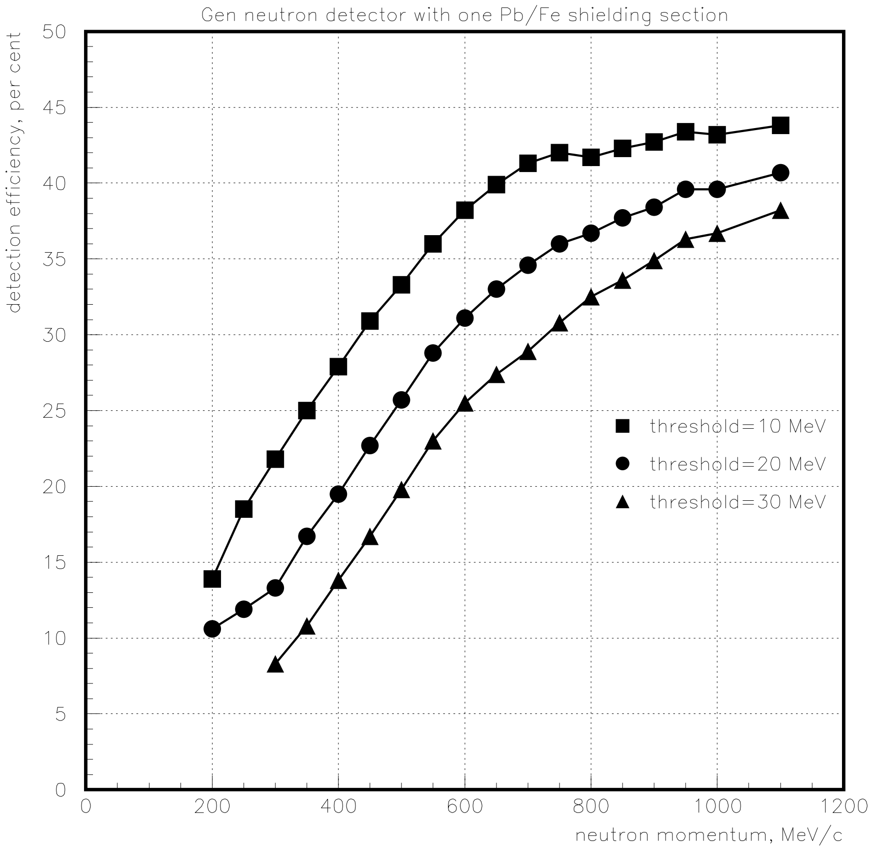


Figure 10: The efficiency of the neutron detector for different threshold levels.

## 4 Inclusive electro-production

In this section the inclusive reactions, which define the singles rates of electrons, pions and kaons in the spectrometers, are presented. In both the BigBite and the neutron arm detectors the rates dominate in the low energy part of the particle spectra. We used a DINREG-based code [27] for the calculation of the low energy part of the inclusive spectra ($E_{hadron} << E_{beam}$). DINREG reproduced published neutron and proton yields in electro-nuclear reactions [28]. DINREG-based calculations for the wire chamber rates were found to be in agreement with measurements in Hall A [30].

The HRS-left will be used to detect negatively charge particles with a momentum of about 3 GeV/$c$, where the single rate is dominated by electrons from deep inelastic scattering (DIS) and photo-produced pions. The yields of negative pions and kaons were calculated by using results from DESY and SLAC measurements of inclusive photo-production [31, 32, 33]. Similar analysis was done for the HRS-right, which will be used for the detection of scattered electrons in the first and third proposed measurements.

### 4.1 Kinematics and definitions

The kinematic quantities of electro-production are presented in Fig. 11.

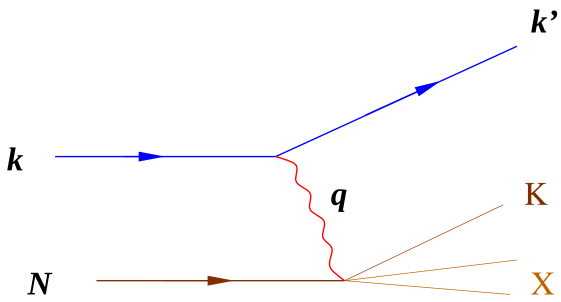


Figure 11: Kinematics quantities for description of electron-nucleon scattering: $k$ and $k'$ are the four-momenta of incoming and outgoing electrons, $N$ is the four-momentum of a nucleon with mass $M$. The exchange photon transfers four-momentum $q = k - k'$ to the target.

The definitions of the kinematical variables are given for the reaction $e + N \rightarrow e' + K + X$. The five four-momenta involved are:

$$
\begin{aligned}
k &= (E, \vec{k}), \text{ for the incident electron} \\
k' &= (E', \vec{k}'), \text{ for the scattered electron} \\
N &= (M, \vec{P}), \text{ for the target nucleon} \\
K &= (E_K, \vec{p}_K), \text{ for the produced kaon} \\
X &= (E_X, \vec{p}_X), \text{ for the residual system}
\end{aligned}
$$

A few kinematic variables are defined below as:

$$q^2 = (k - k')^2 = -Q^2,$$
$$\nu = E - E',$$
$$\epsilon = \left[1 + 2\frac{\nu^2+Q^2}{Q^2} tan^2 \frac{\theta_e}{2}\right]^{-1},$$
$$s = (q + N)^2 = W^2,$$
$$t = (q - K)^2,$$
$$x_F = p^{cm}_{K,z}/p^{cm}_{K,z\,max}, \text{ the Feynman variable}$$

The differential cross section of inelastic $eN$ scattering processes is written in the usual notation as

$$\frac{d^2\sigma}{dE'd\Omega_{e'}} = \frac{\alpha^2}{4E^2 sin^4(\frac{\theta}{2})}\left[W_2(q^2,\nu)cos^2(\tfrac{\theta}{2}) + 2W_1(q^2,\nu)sin^2(\tfrac{\theta}{2})\right].$$

In the approximation of $E, E' >> M_N$ and finite $q^2, \nu$ we will use

$$\frac{d^2\sigma}{dE'd\Omega_{e'}} \approx \frac{\alpha^2}{4E^2 sin^4(\frac{\theta}{2})}\frac{F_2(q^2,\nu)}{\nu}.$$

The differential cross section for the electro-production of hadron $a$ can be presented as:

$$\frac{d^3\sigma}{dE'd\Omega_{e'}d\Omega_K} = \Gamma \cdot \frac{d\sigma_{\gamma^*,K}}{d\Omega_K},$$

where $\Gamma$ is the virtual photon flux factor, given by:

$$\Gamma = \frac{\alpha}{2\pi^2}\frac{E'}{E}\frac{s-M^2}{2MQ^2}\frac{1}{1-\epsilon},$$

and $\frac{d\sigma_{\gamma^*,K}}{d\Omega_K}$ is the cross section for kaon production by the virtual photon. At small scattering angle, where $Q^2 << \nu^2$, only transverse terms of the cross section contribute, so we will use the form:

$$\frac{d\sigma_{\gamma^*,K}}{d\Omega_K} = \frac{d\sigma_T}{d\Omega_K} + \epsilon\,\frac{d\sigma_{TT}}{d\Omega_K}\,cos(2\phi),$$

where $\phi$ is the angle between the electron scattering plane and the kaon production plane.

In the approximation of limiting fragmentation, the invariant cross section $E\frac{d^3\sigma}{d^3p}$ for the production of $K$ is a function of $x_F$ and $p_\perp^2$ [34]. At a photon energy of 6 GeV the accuracy of such an approximation is estimated on the level of 30% for large $x_F$ and small $p_\perp^2$ [33] (see Fig. 12).

## 4.2 The electron singles rates in HRS

In the present experiment the HRS will be at 6° and the central momentum at 2-3 GeV/$c$. The kinematics for the beam energy of 6 GeV corresponds to $Q^2$ of 0.1-0.2 (GeV/$c$)$^2$. The DIS cross section can used to estimate the rate. It leads to a rate up to 600 kHz for the $\mathcal{L}_{eN}$ of $1.1 \cdot 10^{38}$ cm$^2$s$^{-1}$. A similar estimate can be obtained as mentioned above from the total photo-production cross section and the flux of the virtual photons.

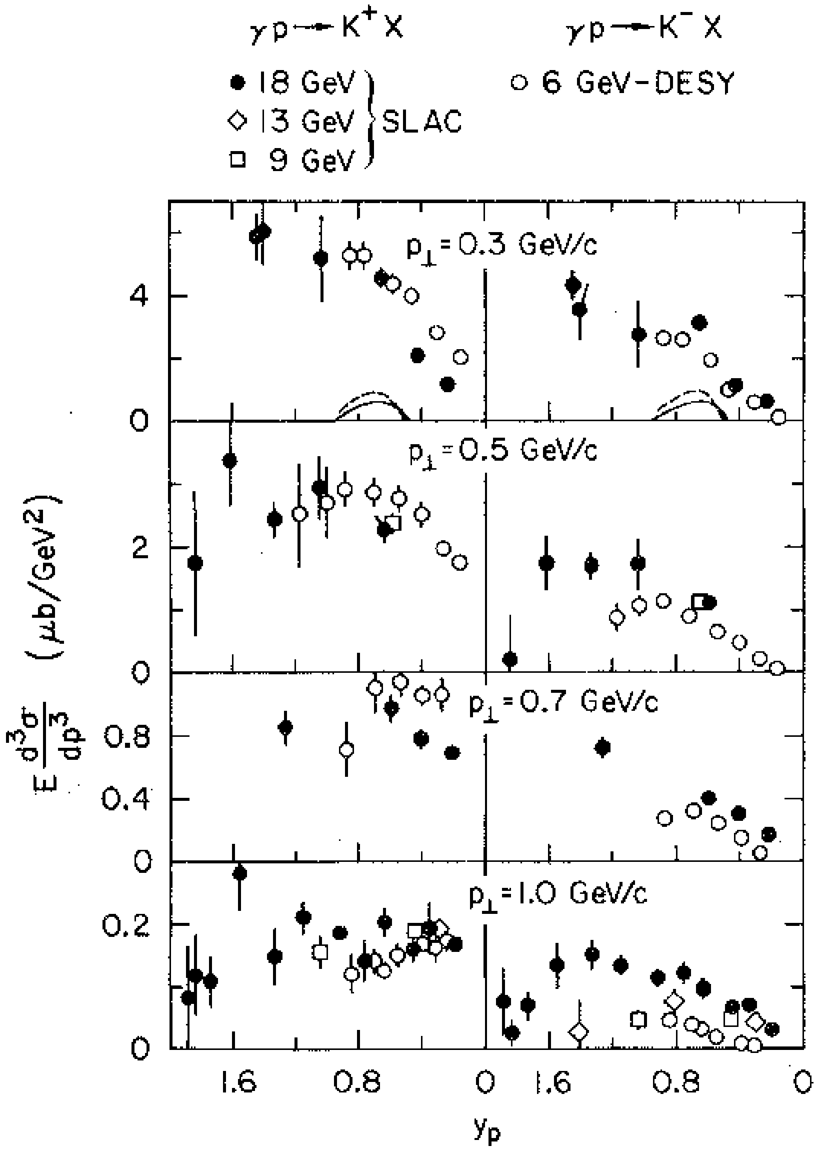


Figure 12: Inclusive kaon photo-production cross section from the proton at different photon energy and perpendicular momenta of the kaon vs. its rapidity [33].

| spectrometer | momentum [GeV/$c$] | electron rate [kHz] |
|---|---|---|
| HRS-left | 3.0 | 600 |
| HRS-right | 2.0 | 240 |

Table 5: The $e^-$ rates for $E_{beam}$ = 6 GeV, $\theta_{HRSs} = 6°$, at $\mathcal{L}_{eN}$ of $1.1 \cdot 10^{38}$ cm$^2$s$^{-1}$.

### 4.3 The pion and kaon rates in HRS

At high beam energy the inclusive processes in the regime of large momentum of the produced hadron can be understood in the framework of the hypothesis of limiting fragmentation [35, 34]. Cross sections are analyzed in terms of Feynman's variable $x_F$ and $p_{\perp}^2$. The experimental results [32, 33] agreed quantitatively with quark model predictions. These data are shown in Fig. 13. For the photon energies of this proposal (4 GeV) the applicability of limiting fragmentation ideas can be justified by the reasonable agreement between high energy results [32, 33] and measurement at $E_\gamma = 3.2$ GeV [31]. To estimate the particle

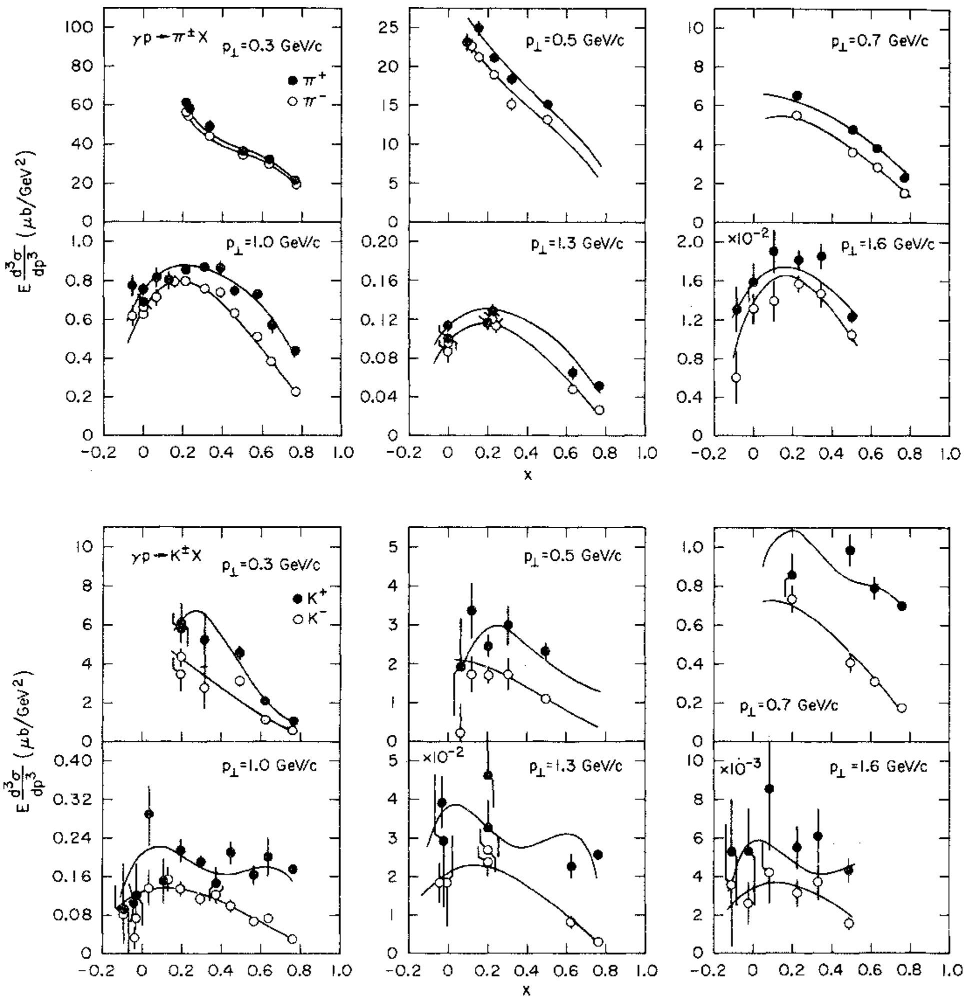


Figure 13: Inclusive pion and kaon photo-production cross section from the proton at different perpendicular momenta vs. Feynman's variable $x_F$ [33].

yields the photon intensity must be calculated. The intensity of the equivalent photon flux in electro-production experiment was calculated according to a prescription [36]. The photon spectra are shown in Fig. 14. The resulting counting rates are shown in the Tab. 6.

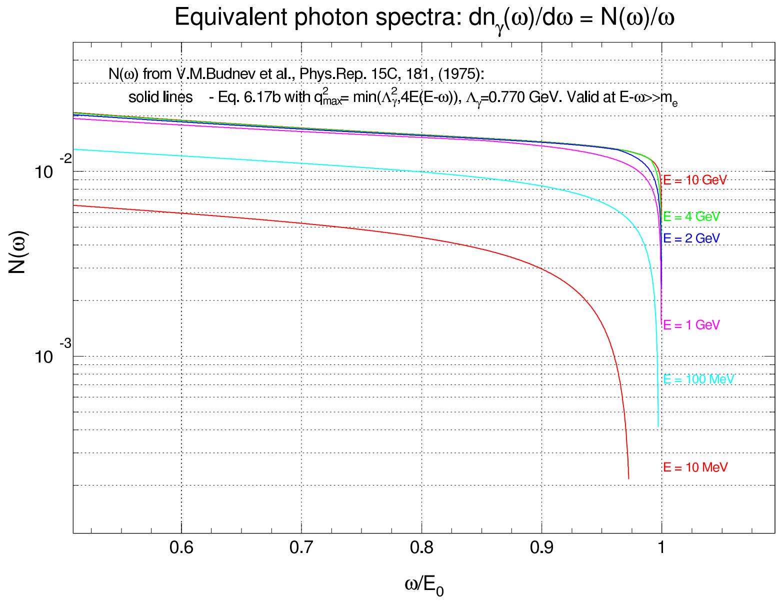


Figure 14: The photon spectra according to Budnev [36].

| spectrometer | momentum [GeV/$c$] | $\pi^-$ [kHz] | $K^-$ [kHz] |
|---|---|---|---|
| HRS-left | 3.0 | 40 | 0.088 |

Table 6: The $\pi^-$ and $K^-$ singles rates for conditions of Tab. 5.

### 4.4 Coincidence rate between HRSs

In the second measurement both HRS's will be used. The coincidence between them will be used as a DAQ trigger. The rate of real electron-hadron coincidence was estimated from the flux of virtual photons and hadron photo-production cross section as was described above in this section. The aerogel counter A1 in the HRS-left can provide an on-line rejection factor of 100 for the $e^-$ and $\pi$, which will maintain the DAQ rate at low level of 10 Hz. (see Tab. 7).

| event type | $e\pi^-$ rate [Hz] | $eK^-$ rate [Hz] |
|---|---|---|
| real coinc. | 85 | 1.2 |
| accid. coinc. | 480 | 0 |

Table 7: The $\pi^-$ and $K^-$ real and accidental coincidence rates of the HRSs for conditions of Tab. 5.

### 4.5 Singles rates in the BigBite

The proposed configuration of the detectors was analyzed for singles rates, which defined the maximum usable luminosity and possible production rate. This section deals with the calculation and measurement of the singles rate in the BigBite spectrometer for both parts of proposed experiment.

Figure 15 shows the expected rate of electrons at different momenta. The proton rates are shown in Fig. 16. To cross check these calculations we made a measurement of the counting rate of a multi-wire proportional chamber located behind BigBite at 65° and a distance of 8 m from the target. During measurements the beam energy was 4.2 GeV. The observed rate was found to be about half the calculated rate [30]. In the analysis below we used the calculated rate as a conservative estimate of the background.

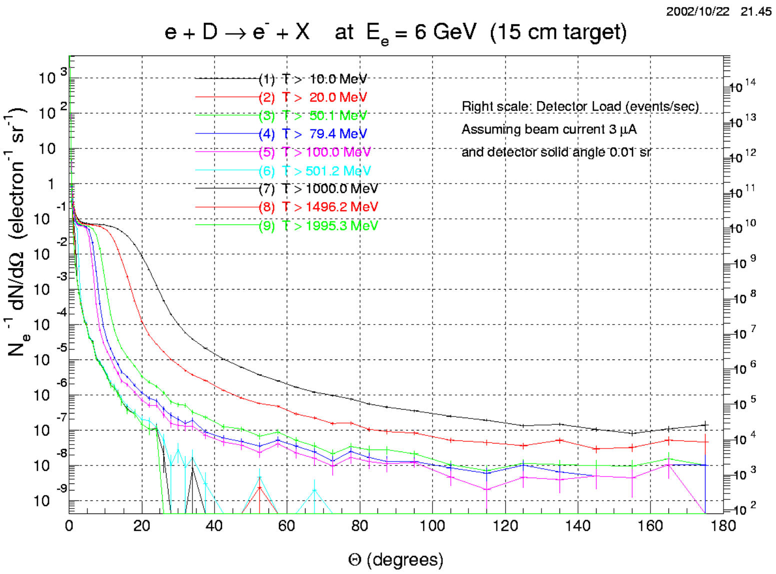


Figure 15: Electron rate at $\mathcal{L}_{eN}$ of $2.75 \cdot 10^{37}$ cm$^2$s$^{-1}$. The detector solid angle is 0.01 sr in this plot.

For the first measurement, BigBite will be installed out of plane at a polar angle 27°, at larger than the nominal distance from the target, so the solid angle will be 38 msr. The rates integrated over the acceptance are shown in the Tab. 8.

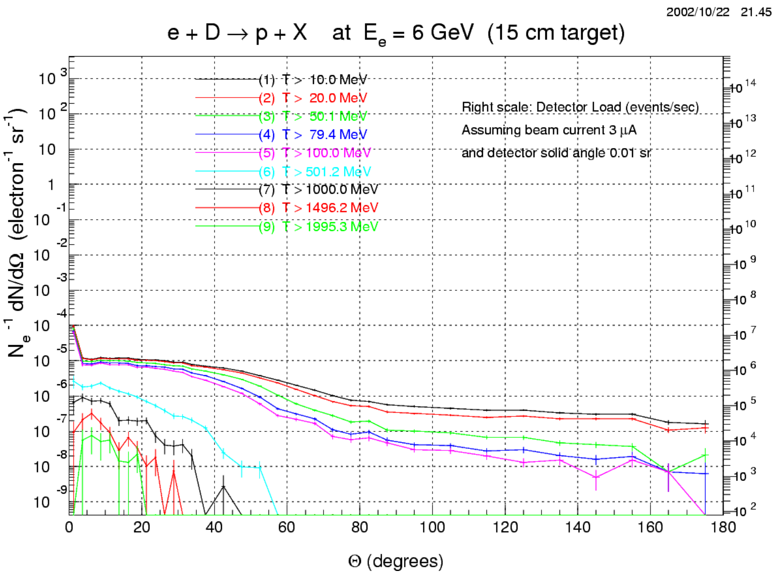


Figure 16: Proton rate at $\mathcal{L}_{eN}$ of $2.75 \cdot 10^{37}$ cm$^2$s$^{-1}$. The detector solid angle is 0.01 sr in this plot.

| Field of 9 kG | $e^-$ | $\pi^\pm$ | proton |
|---|---|---|---|
| rate [MHz] | 0.10 | 2.2 | 1.1 |

Table 8: The singles rates in BigBite at $\mathcal{L}_{eN}$ of $1 \cdot 10^{37}$ cm$^2$s$^{-1}$ for the configuration of first measurement.

In the second measurement, BigBite will be installed at 70° and used for the detection of the soft protons with momenta 150-300 MeV/$c$. Ionization density for soft protons will be about 10-20 times higher that for background electrons and pions. This allows us to reduce the high voltage on the drift chambers and make them sensitive primarily to these slow protons. Other particles will contribute only to the rate of the scintillator counters which have high rate performance and segmentation. In the second measurement, the BigBite information will be used in off-line analysis only. Table 9 shows expected particle rates in BigBite during the second measurement. Independent estimate of the soft proton rate was done by using the deuteron photo-disintegration cross section and the intensity of the low energy photons based on the article [36].

| Field of 7 kG | $e^{\pm}$ | $\pi^{\pm}$ | proton |
|---|---|---|---|
| rate [MHz] | 6.8 | 13.6 | 6.8 |

Table 9: The singles rates in BigBite at $\mathcal{L}_{eN}$ of $1.1 \cdot 10^{38}$ cm$^2$s$^{-1}$ for the second measurement.

### 4.6 Singles rate in the neutron detector

In the proposed experiment we will use the neutron detector N-200, which is under preparation for the GEN experiment E02-013 [21]. In 2002 we built a 10% segment of the full detector (20 neutron bars and 8 veto paddles) and used it for measurement of the singles rates and trigger rates at a distance of 8 m from the target and 25° from the beam line. Rates were found to be in reasonable agreement with DINREG-based calculations [29].

Figure 17 shows the expected rate of pions at different momenta, which contribute to the rate in N-200. The rate of neutrons is shown in Fig. 18. Table 10 shows the expected detectors rates in N-200 during the first measurement.

| | veto paddle | N-bar PMT, above 5 MeVee | trigger, above 20 MeVee |
|---|---|---|---|
| rate [MHz] | 0.40 | 0.02-0.06 | 1.9 |

Table 10: The rates in the neutron detector at $\mathcal{L}_{eN}$ of $1 \cdot 10^{37}$ cm$^2$s$^{-1}$ for the first measurement.

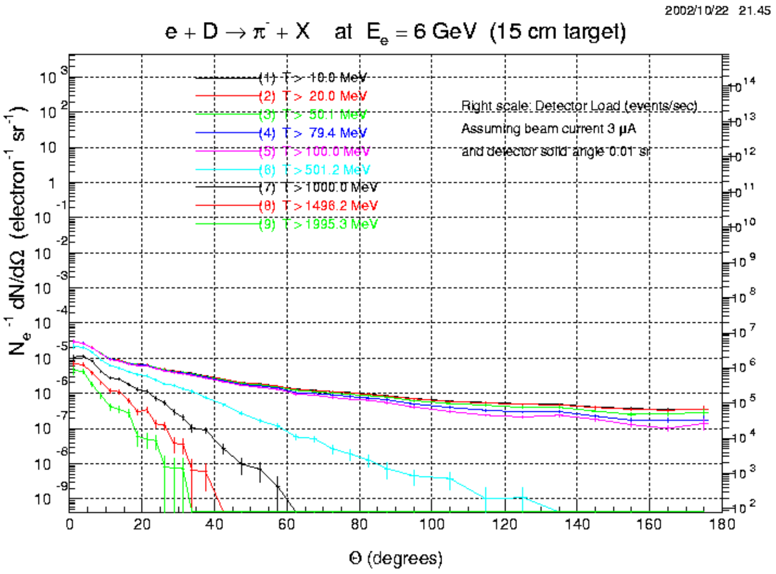


Figure 17: Pion rate at $\mathcal{L}_{eN}$ of $2.75 \cdot 10^{37}$ cm$^2$s$^{-1}$. The detector solid angle is 0.01 sr in this plot.

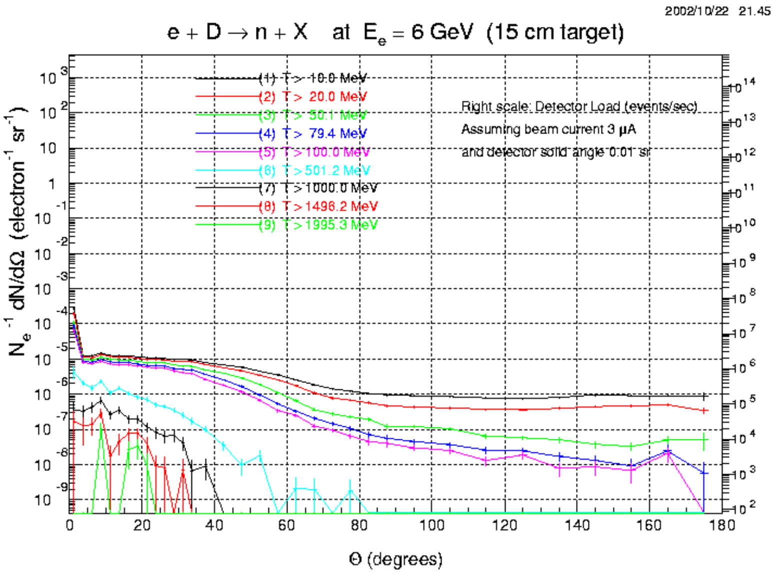


Figure 18: Neutron rate at $\mathcal{L}_{eN}$ of $2.75 \cdot 10^{37}$ cm$^2$s$^{-1}$. The detector solid angle is 0.01 sr in this plot.

## 5 Proposed measurements

Three separate measurements are proposed. **The first** will allow observation of a narrow $\Theta^+$ state in an invariant mass spectrum and collect an angular distribution of the decay products. **The second** will allow observation a $\Theta^+$ state in a missing mass spectrum over a wide range of masses, to perform an accurate measurement of the mass value, and to find the linear polarized photon asymmetry. **The third** measurement is designed to search for the $\Theta^+$ state's partners in the antidecuplet and in the tensor multiplet; we will find them or put a very strict upper limit on the photo-production cross section. The key experimental elements of the present proposal are

- tagging on a high momentum kaon produced by a photon;
- a concept of post-target photon tagging;
- an assumption of the diffractive mechanism of $\Theta^+$ production;
- a pair of high resolution spectrometers HRS in Hall A;
- a pair of novel septum magnets for HRS, which allow detection of particles for the central trajectory in each spectrometer at an angle of 6°;
- a large acceptance magnetic spectrometer BigBite, with a high resolution detector package under construction for the GEN experiment;
- a large array of the neutron counters, which is also a part of the GEN experimental setup;
- a 50 cm long cold gas Deuterium target;
- the experimental data on forward angle kaon photo-production [31, 32, 33].

The high energy forward negative kaon presents a very important **tag**, which reduces dramatically the contribution of competing reactions into $K^+$-neutron event sample. The post-target tagging approach, often used in hyper-nuclei experiment, is a low $Q^2$ electro-production study of photo-production processes. Because the HRS spectrometer momentum resolution (rms) is about $1.1 \cdot 10^{-4}$ such tagging has unique resolution. The effective flux of photons is also much higher than achievable with a tagged real photon beam if the electron scattering angle is sufficiently small. The photo-production mechanism of the $\Theta^+$ is unknown. However, it is logical to expect that it is similar to the $t$-channel dominated process for producing the $\Lambda(1520)$. The important parameters to measure in this case are the total cross section and its $t$-dependent slope. The cross section may also have a $\sigma_{TT}$ term, where the ratio to the $\sigma_T$ is related to the $\Sigma$ photon polarization observable and can be estimated from this experiment because of significant out-of-plane acceptance. For small scattering angles the effective degree of linear photon polarization can be presented as $(1+E_\gamma^2/(2E_e^iE_e^f))^{-1}$ which is ≈60% for the conditions of the M2 measurement.

The measurements will use a 50 cm long cold gas Deuterium or Hydrogen target. An alternative target in the first measurement is a set of thin and narrow foils of Beryllium or Carbon.

## 5.1 The invariant mass experiment (M1)

We are going to study the reaction $n(\gamma, K^- n K^+)$. The concept of the measurement is shown in Fig. 2. An electron beam with a current of 20 $\mu$A at an energy of 4.5 GeV will be used. The density of gas will be adjusted to obtain the $\mathcal{L}_{eN}$ of $1 \cdot 10^{37}$ cm$^{-2}$s$^{-1}$. The negative kaon will be detected in the magnetic spectrometer HRS-left at a central angle of 6° with a septum magnet. The positive kaon will be detected in the BigBite spectrometer at horizontal/vertical angles 18°/-15°, and the neutron will be detected in the large neutron detector at horizontal/vertical angles 18°/+22°. The invariant mass resolution (FWHM) is about 2.9 MeV. If an actual resonance width is found less than 2 MeV, the experiment can be continued with the HKS spectrometer [26] for detecting the $K^+$, where the mass resolution (FWHM) will be of order 2 MeV, however the counting rate will be less, an angular coverage and the range of invariant mass much smaller.

### 5.1.1 The MC simulation

The distributions shown below are generated from MC simulated data, in which a 3 MeV width of the resonance was assumed. The statistics corresponds to 20 days of data collection with the production cross section of 50 nb at luminosity of $1 \cdot 10^{37}$ cm$^{-2}$s$^{-1}$. A momentum resolution for BigBite of 0.6% and time resolution for the neutron arm of 0.4 ns were used in calculations. The rms of the instrumental resolution is 1.3 MeV. Figure 19 shows the invariant mass distribution and an instrumental resolution. At the peak inside the width of $\Gamma = 4.2$ MeV the estimated ratio of the signal to the background is about 3.6. The background mainly consists of real coincidence events. Measuring the angular distribution of the $K^+$n in the cm system may allow us to establish the spin of the $\Theta^+$. The angular distribution for the $J = \frac{1}{2}$ is isotropic, but in case of the $J = \frac{3}{2}$ it can vary. Figure 20 shows the distributions of MC simulated events over the cosine of the angle between the $K^+$ and the $\Theta^+$ in the $\Theta^+$ rest frame. The plot shows two distributions. The solid line shows the case of the uniform distribution in the cm frame deformed by the acceptance of the detector system, the dotted line shows the case of $J = \frac{3}{2}$ if there is a dominance of the substates $M = \pm\frac{1}{2}$. The extra weight of the $M = \pm\frac{1}{2}$ component will be determined with an accuracy of 0.1. The distribution over four-momentum $t$ ranges from -0.10 to -0.20 (GeV/$c$)$^2$, which can be used for initial estimation of the slope B of $t$ dependence with an accuracy of $\pm 1.6$ (GeV/$c$)$^2$. Figure 21 presents distributions over the incident photon energy, the resonance momentum, the neutron momentum, the positive kaon momentum, and the correlation of the neutron and kaon momenta. One of the results of this MC is a value of probability ($P_a$) to have all three particles (a negative kaon, a positive kaon, and a neutron) in the acceptance of their arms. The value of $P_a$ was found about $1.7 \cdot 10^{-4}$ for the configuration under discussion.

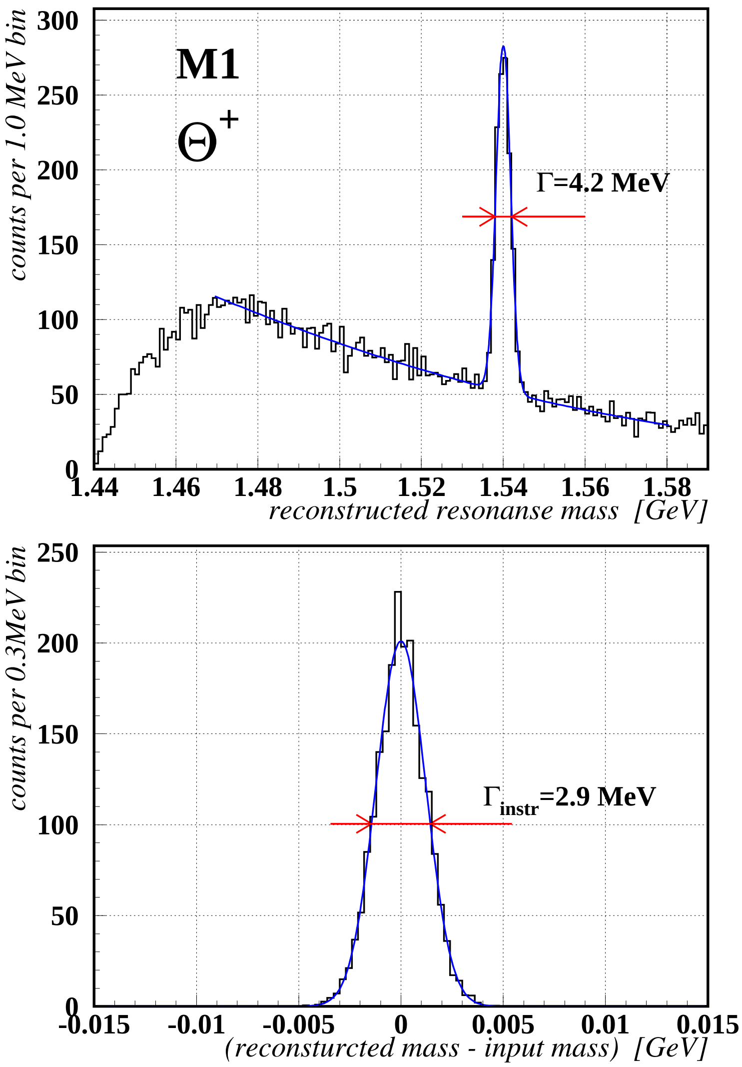


Figure 19: The distribution over invariant mass of the $nK^{+}$ system and the instrumental resolution in the reaction $\gamma n \to K^{-}\Theta^{+} \to K^{-}K^{+}n$.

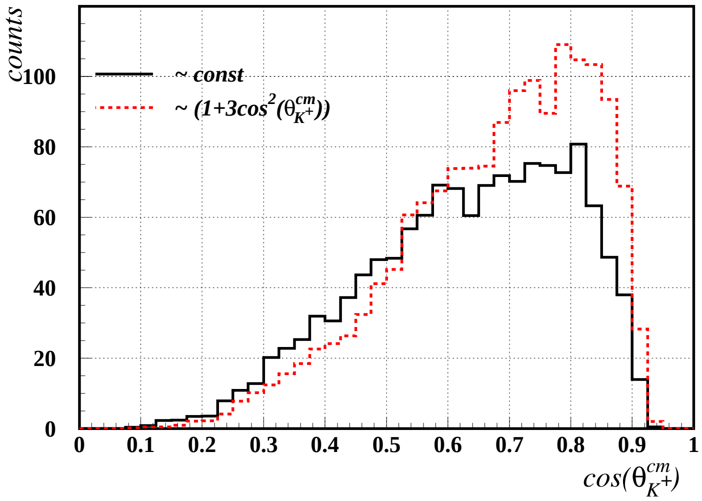


Figure 20: The event distributions over angle between the K$^+$ and the $\Theta^+$ in the $\Theta^+$ rest frame. The solid line corresponds to the case of the uniform distribution, the dotted line shows the event distribution in the case $J = \frac{3}{2}$ and $M = \pm\frac{1}{2}$.

#### 5.1.2 The calculation of the $\Theta^+$ production rate

In calculating the $\Theta^+$ production rate we used the value of total photo-production cross section of 50 nb as an estimate based on information from CLAS experiment (60-160 nb) [38] and the photo-production cross section [39], which gives 130 nb at a photon energy of 4 GeV. The value 130 nb agrees with the only presently published result of 200 nb at 1.7-2.5 GeV [7]. We took into account a 50% branching ratio for the decay to $nK^+$. We assumed the resonance width (FWHM) of 3 MeV. For the parameter of the $t$ dependence of the $K^-$ angular distribution we used a conservative value of 3 (GeV/$c$)$^{-2}$, which is much less than the known slope of 6 (GeV/$c$)$^{-2}$ for the $\Lambda(1520)$. We have found that for the detectors in this proposal the resulting production rate is almost the same for slope values between 2 and 6 (GeV/$c$)$^{-2}$. The photon-neutron luminosity was calculated as

$$\mathcal{L}_{\gamma n(eutron)} = \frac{N}{A} \cdot 0.015 \cdot \frac{\Delta E_\gamma}{E_\gamma} \cdot \mathcal{L}_{eN} \sim 5.25 \cdot 10^{-4} \cdot \mathcal{L}_{eN} \;=\; 5.25 \cdot 10^{33}\ \mathrm{cm}^{-2}\mathrm{s}^{-1},$$

where $E_\gamma$ and $\Delta E_\gamma$ are defined by the kaon momentum and its range accepted in HRS-left, $< E_\gamma >= 4.0$ GeV and $\Delta E_\gamma = 0.28$ GeV; $\mathcal{L}_{eN}$ is the electron-nucleon luminosity, $\mathcal{L}_{eN} = 1 \cdot 10^{37}$ cm$^{-2}$s$^{-1}$. Such a value of $\mathcal{L}_{\gamma n(eutron)}$ is about $10^3$ times higher than what one can obtain with real-photon tagging. This leads to the production rate

$$\nu^{\Theta^+}_{\gamma,K^- nK^+} = \mathcal{L}_{\gamma n} \cdot \sigma^{\Theta^+}_{\gamma n} \cdot f^{HRS}_{\gamma,K^-} \cdot f_{nK^+} \cdot f^{decay}_{K^-} \cdot \eta_n \cdot f^{decay}_{K^+} \cdot b_{nK^+} \;=\; 55 \text{ events per day},$$

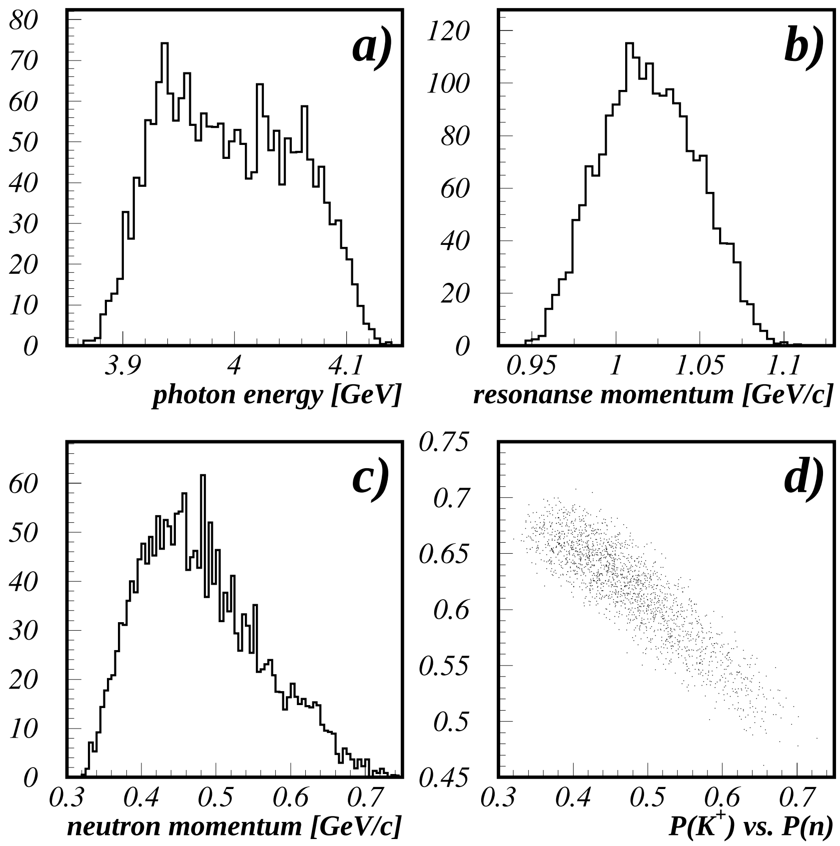


Figure 21: The event distributions a) the photon energy spectrum; b) the $\Theta^+$ momentum; c) the final neutron momentum; and d) the correlation between the neutron and kaon momenta.

where $\sigma_{\gamma n}^{\Theta^+}$ is the cross section of 50 nb; the $f_{\gamma,K^-}^{HRS}$ is a fraction of $K^-$ associated with $\Theta^+$ production within HRS angular and momentum acceptances, it is ≈0.034; $f_{nK^+}$ is a fraction of $\Theta^+$ events when both decay products are in angular acceptance of BigBite and N-arm detectors, $f_{nK^+}$ is ≈0.005; $f_{K^-}^{decay} = 0.33$ is the survival probability of a $K^-$ after a 25 meter path in the HRS; $\eta_n = 0.24$ is the detection efficiency of the neutron; $f_{K^+}^{decay} = 0.36$ is the average survival probability of $K^+$ after flight of a 5 meter path from the target to the BigBite trigger detector; and $b_{nK^+}$ is the branching ratio for $\Theta^+$ decay to $nK^+$, $b_{nK^+} = 0.5$. The actual rate $\nu_{\gamma,K^- nK^+}^{\Theta^+}$ may be higher or smaller depending upon the cross section.

#### 5.1.3 The singles and correlated rates

The singles rates in the HRS, BigBite, and the neutron detector were calculated based on the analysis presented in Sec. 4. For the luminosity proposed for the first measurement the rates are presented in Tab. 11.

| detector | momentum | rate [kHz] | rate [kHz] | rate [kHz] |
|---|---|---|---|---|
| HRS-left | 3.0 GeV/$c$ | $\nu_e$=55 | $\nu_{\pi^-}$=4.0 | $\nu_{K^-}$=0.008 |
| BigBite | >0.10 GeV/$c$ | $\nu_e$=100 | $\nu_{\pi^\pm}$=2200 | $\nu_p$=1100 |
| N-arm | $A_{sum}$ >20 MeVee | $\nu_n^{trig}$=200 | $\nu_{p,\pi^\pm}^{trig}$=1700 | |

Table 11: The singles rates in the HRS, the BigBite and N-arm at $\mathcal{L}_{eN}$ of $1 \cdot 10^{37}$ cm$^{-2}$s$^{-1}$ for the configuration of the first measurement.

The correlated rate due to real coincidences between the HRS-left, BigBite, and the neutron detector was estimated from inclusive $K^-$ rate and a phase space for the $nK^+$ system with the assumption that it has isotropic decay in cm system. Such an estimate is about 10 times higher than the $\Theta^+$ production rate, but non-resonance events are distributed over a wide range of invariant mass (see Fig. 19). Additional correlated rate on trigger level is due to misidentification of the particles in the detectors. For example in the on-line HRS's event sample will have about 50% of $\pi^-$, in almost all BigBite events there are the pions and protons, the neutron detector trigger rate is dominated by charged pions.

#### 5.1.4 Trigger rate and event analysis

The trigger will use a single trigger of HRS-left. The on-line rejection factor of the electrons in the HRS is about 1000 based on the combination of shower detector and aerogel Čerenkov counter. On-line rejection of pions in the HRS is about 100 based on the A1 aerogel Čerenkov counter. The trigger rate estimate is of order 100 Hz. The rate of BigBite scintillator trigger plane is expected to be on the level of 3 MHz. In case of unexpectedly high rate in HRS the experiment will use HRS-BigBite coincidence with an 50 ns time window, which will provide a reduction of the trigger rate by a factor of 6.

Off-line analysis should allow us to obtain a higher rejection factor of pions and electrons in HRS by means of the RICH by at least by a factor of 10. Off-line analysis of BigBite time-of-flight and water and aerogel Čerenkov amplitudes will give rejection factors on the level of 1000 for protons and pions (see for performance of the water Čerenkov counter [26]). The check of the event vertex in the target provides an additional factor of 10 for the rejection of accidental events. Off-line analysis of the neutron arm veto information will allow us to reduce pion/proton contribution into the trigger rate by a factor of 50. The remaining rate of the neutron arm trigger, mostly from neutrons, will be at the level of 200 kHz. The accidental coincidence rate between HRS+BigBite and the neutron arm, within 100 ns time window for neutrons, will be on the order of $10^{-5}$ Hz. These events will make a very small background in the invariant mass spectra distributed in a 100+ MeV wide region. For non-resonance real coincidence event rate, as it was discussed before, the upper limit can be estimated from HRS-left inclusive $K^-$ rate and acceptance of the detectors for $nK^+$. This rate is about 0.0035 Hz. The expected $\Theta^+$ state production rate of 0.00064 Hz will be concentrated in a region of 4.2 MeV. A good ratio (signal/background of 4/1) provides sufficient insurance for the case that the actual photo-production cross section is even smaller than assumed in our estimation. The rejection factors used above are quite conservative as well.

### 5.2 The missing mass experiment (M2)

An electron beam with a current of 110 $\mu$A at an energy of 6 GeV will be used. The density of gas will be adjusted to obtain the $\mathcal{L}_{eN}$ of $1.1 \cdot 10^{38}$ cm$^{-2}$s$^{-1}$. As was suggested above, the negative kaon will be detected in the magnetic spectrometer HRS-left at a central angle 6° with a septum magnet. The scattered electron will be detected in the magnetic spectrometer HRS-right at central angle 6° with the second septum magnet. The soft proton will be detected in the BigBite spectrometer at a central angle of 70°.

In this measurement the resonance will remain undetected, but observed in the missing mass spectra in the reaction $\mathrm{D}(e, e'K^- p_{soft})\mathrm{X}$ . It requires detection of the electron, the negative kaon, and the proton. To achieve sufficient counting rate in this approach we rely on the detection of a very soft proton. The number of such protons can be calculated from the spectral function for the deuteron, which is shown in Fig. 22. For example, the fraction of protons with momentum above 200 MeV/$c$ is 6.8%. In addition to the events related to the spectator protons we estimate, that a similar number of events will be related to the re-scattering of the proton, kaon and $\Theta^+$ particle. The measurement of the proton spectra will provide information about the reaction mechanism and may be even hint at the cross section of the proton-$\Theta^+$ scattering. The technique for detecting the soft proton was recently developed for the ChPT E01-014 experiment [20], based on the BigBite spectrometer. The ChPT experiment was designed for a proton momentum above 180 MeV/$c$. With the long cold gas target proposed here the threshold can be lowered to 150 MeV/$c$. In the deuteron, there are 13.5% protons with momenta above 150 MeV/$c$. Detection of the scattered electron provides the opportunity to observe the linear polarization photon asymmetry by using the event distribution over the out-of-plane angle between the electron scattering and the $K^-$ production planes. According to recent predictions [40, 41], this observable has a strong sensitivity to the $\Theta^+$ parity.

#### 5.2.1 The MC simulation

The Monte Carlo simulation of this setup was also done in the framework of GEANT-3. The results were confirmed by analytical calculations. The probability for the negative kaon to be in the angular acceptance of HRS-left in this measurement is about 5%, which is even larger than in the first measurement because the virtual photon direction is closer to HRS-left. The probability of soft proton detection with momentum above 150 MeV/$c$ was found from effective solid angle of BigBite for extended target. For a nominal length of the target of 50 cm and BigBite angle of 70°, the average solid angle is 86 msr. The fraction of protons in the deuteron with momentum above 150 MeV/$c$ ($P_{150}$) was found from the distribution shown in Fig. 22 as

$$P_{150} = \int\limits_{150}^{\infty} n(p)\, p^2\, dp \Big/ \int\limits_{0}^{\infty} n(p)\, p^2\, dp$$

We estimated from the value of the $K^-p$ elastic cross section that probability to find proton in the reaction D$(e, e'K^-p_{soft})$X with momentum above 150 MeV/$c$ can be higher than $P_{150}$ by a factor of 1.3. The momentum and angular resolutions of BigBite for a soft proton was found from an additional MC simulation, which includes all elements of the setup (see results in Tab. 12). For a proton with momentum of 150 MeV/$c$ a relative resolution about 1.7% is obtained. The missing mass spectra and instrumental resolution are shown in Fig. 23. The instrumental resolution (rms) is of 1.5 MeV. Figure 24 shows event distributions over $t$ four-momenta and difference $t - t_\circ$, where $t_\circ$ is a minimum value of $t$ corresponded to zero angle between the $K^-$ and the virtual photon momenta. Recently two calculations [40, 41] have found a large difference in the polarized photon asymmetry for the cases of the positive and negative parity of the $\Theta^+$ state. The result [41] for the 4 GeV photon energy is about -0.2 for the positive parity and -0.8 for negative one. The value of the asymmetry has dependence on the angle between $K^-$ and photon momenta. At zero angle, where $t = t_\circ$, the asymmetry is zero. Preliminary value of the asymmetry averaged over acceptance of our experiment (see Fig. 24) is about -0.71 of it's maximum value. The events distribution over out-of-plane angle of $K^-$ in the proposed experiment is shown in Fig. 25 for the case of the $\sigma_{TT}/\sigma_T = 0$ and in Fig. 26 for the case of the $\sigma_{TT}/\sigma_T = -0.71$. The difference between expected raw asymmetries (it includes the factors of 60% photon polarization and backgound dillution) in two cases of the $\Theta^+$ parity is about -0.33*0.75=0.25, which allow for 5 sigma significance of the result.

#### 5.2.2 The $\Theta^+$ events rate

The estimation of the production rate is quite similar to that shown above for the first measurement. The detector configuration in the second measurement allows us to use much

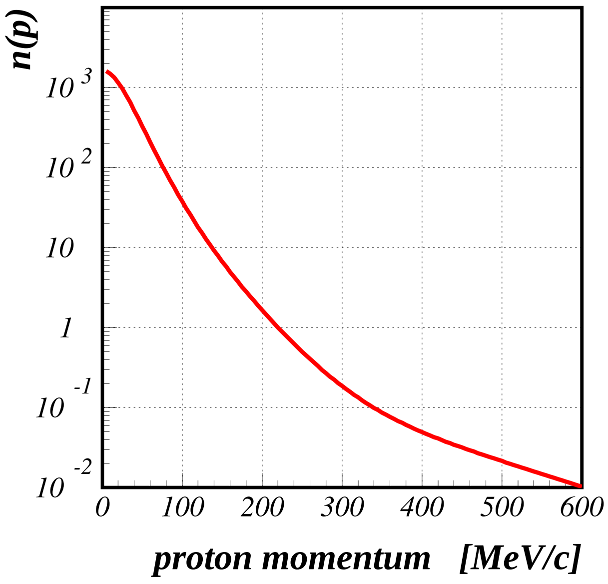


Figure 22: The proton spectra function in deuteron [37].

| momentum $p$ [MeV/$c$] | $\sigma_p/p$ [%] | $\sigma_{\theta,in\,plane}$ [mr] | $\sigma_{\theta,out\,plane}$ [mr] | z vertex resolution [cm] |
|---|---|---|---|---|
| 140 | 1.9 | 16.5 | 13 | 4.5 |
| 160 | 1.5 | 14.0 | 10 | 3.7 |
| 180 | 1.2 | 12.5 | 8 | 2.9 |
| 200 | 1.1 | 11.0 | 6 | 2.4 |
| 220 | 1.0 | 10.0 | 5 | 2.2 |
| 240 | 0.9 | 9.4 | 5 | 2.0 |

Table 12: The resolutions of the BigBite spectrometer for soft protons in the proposed experiment.

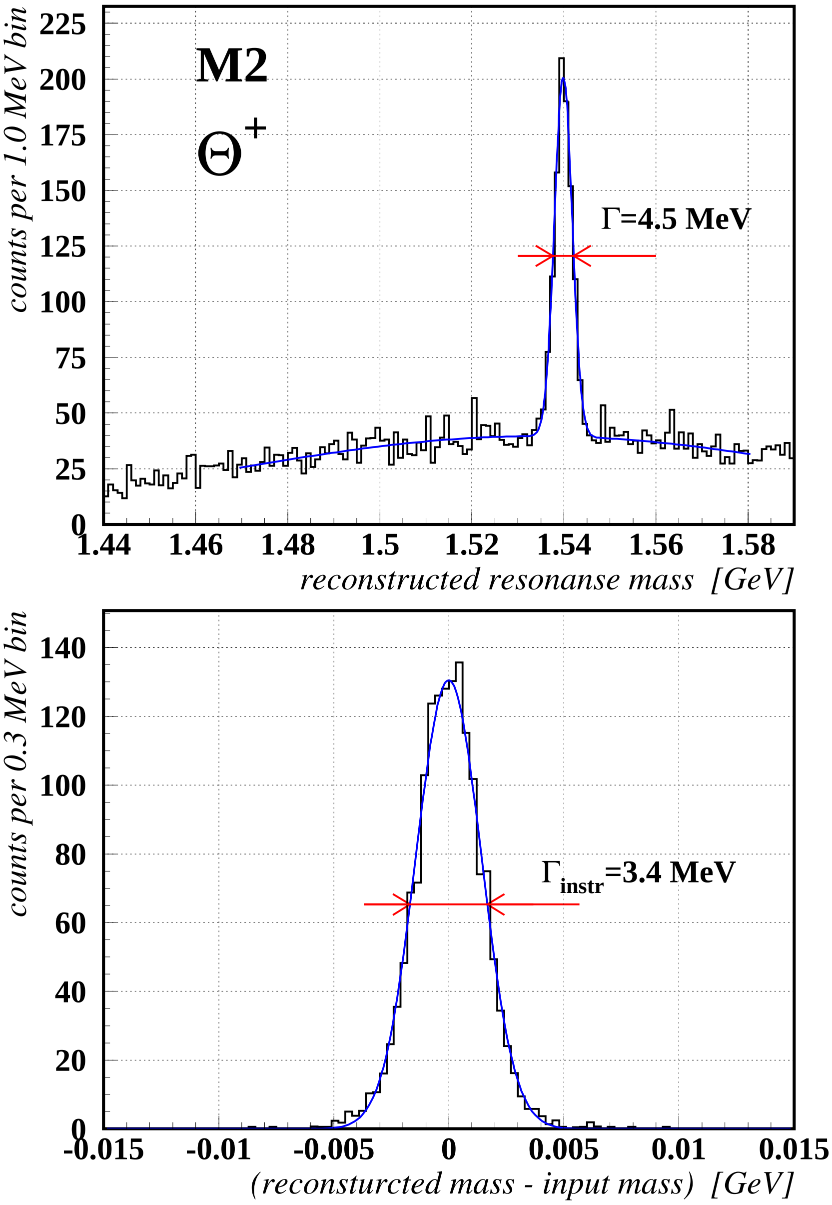


Figure 23: The distribution over missing mass and the instrumental resolution in the second measurement. The peak corresponds to the resonance width 3 MeV combined with an instrumental resolution (FWHM) = 3.4 MeV. Background level is an accidental coincidences at the $\mathcal{L}_{eN}$ of $1.1 \cdot 10^{38}$ cm$^{-2}$s$^{-1}$.

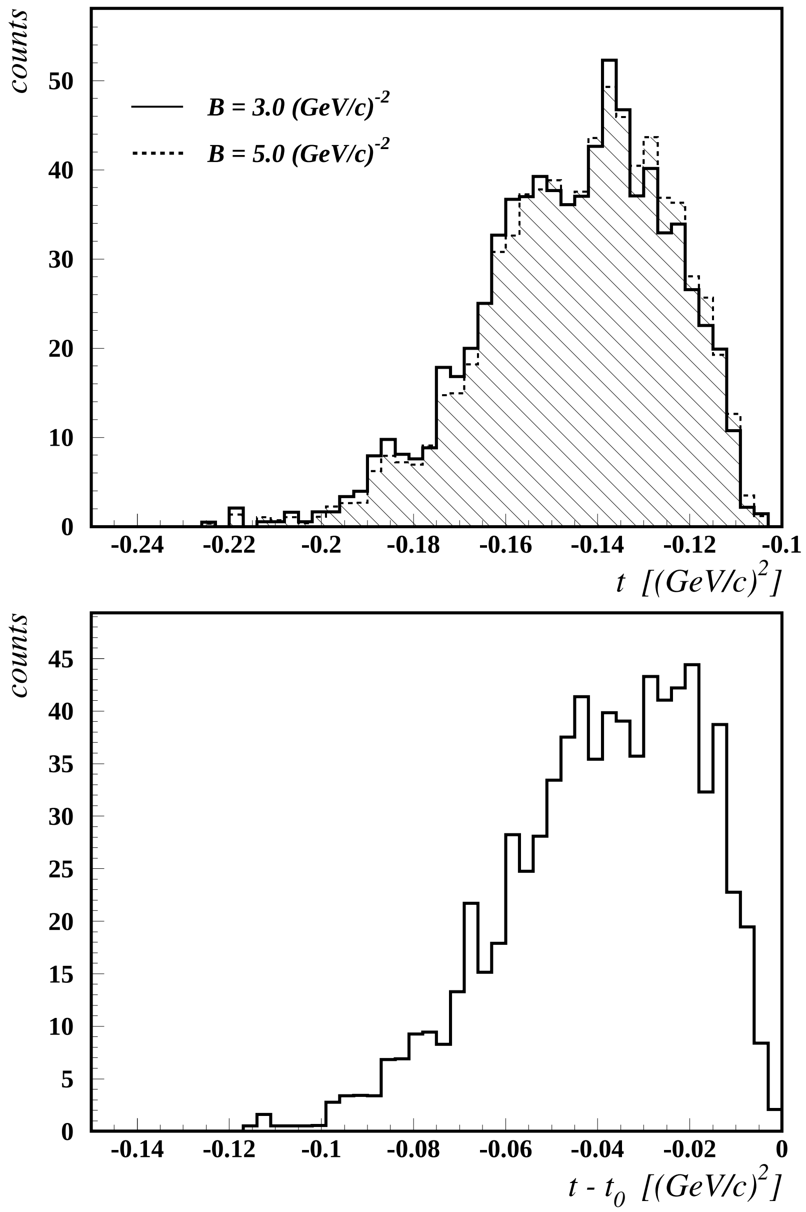


Figure 24: The range of $t$ four-momenta expected in the second measurement. Two distributions are for different assumptions about the value of the slope for $t$-dependence of the cross section. Bottom plot shows a distribution over difference $t - t_\circ$, where $t_\circ$ is a minimum value of $t$ corresponded to zero angle between the $K^-$ and the virtual photon momenta.

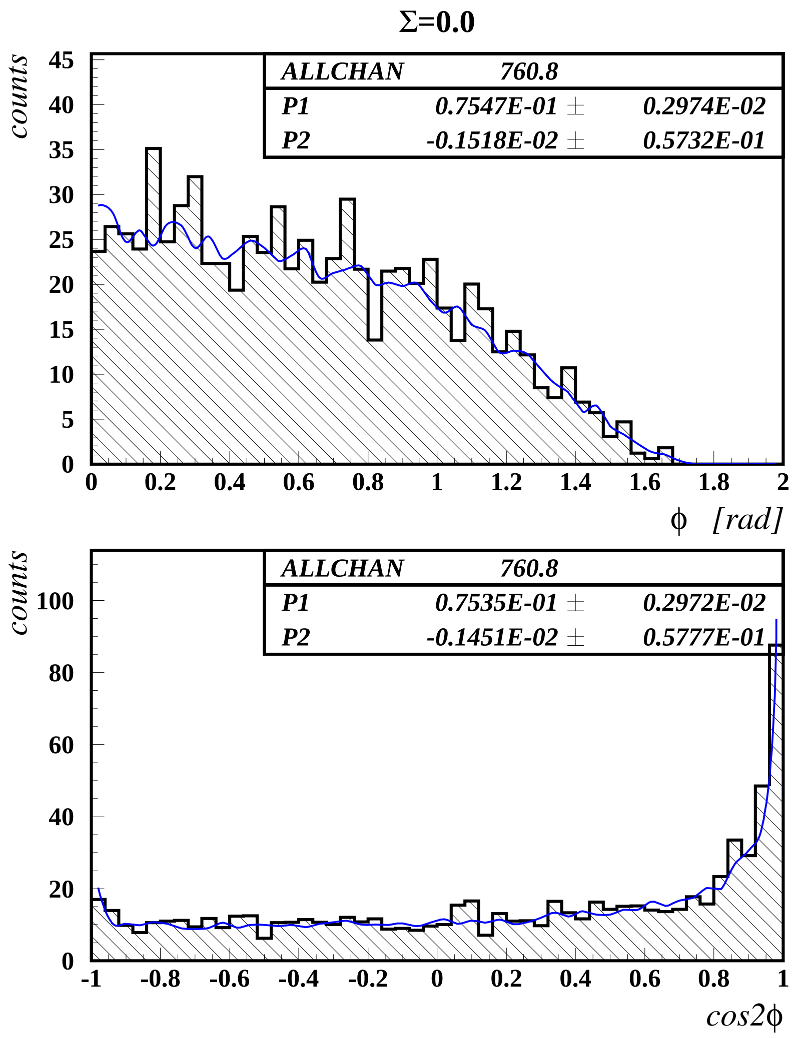


Figure 25: The event distribution over $K^-$ out-of-plane angle for the zero value of the polarized photon asymmetry.

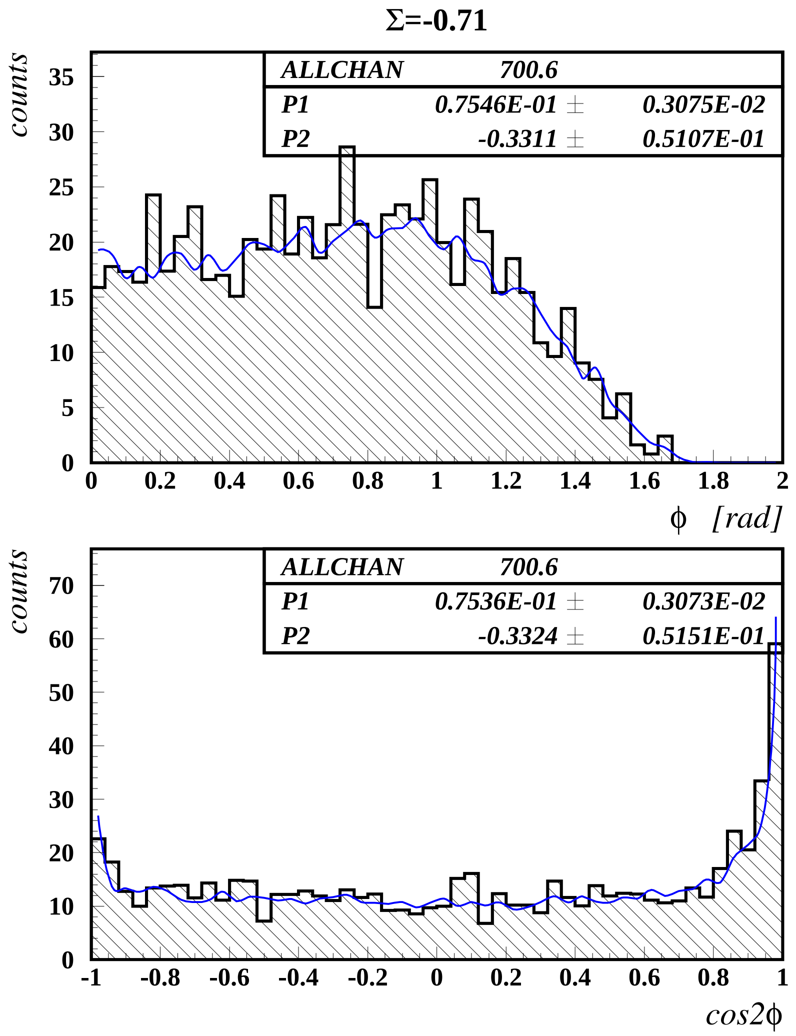


Figure 26: The event distribution over $K^-$ out-of-plane angle for the value of the polarized photon asymmetry of -0.71. The experimental asymmetry is of -0.33 due to 60% photon polarization, real and accidental background. An accuracy of the asymmetry measurement (sigma) is 0.052.

higher luminosity. The calculations for the production and background are made for the $\mathcal{L}_{eN}$ of $1.1 \cdot 10^{38}$ cm$^{-2}$s$^{-1}$. The virtual photon-neutron luminosity was calculated as (see definitions in Sec. 4)

$$\mathcal{L}_{\gamma^* n(eutron)} = \frac{N}{A} \frac{\alpha}{2\pi^2} \frac{E'}{E} \frac{E-E'}{Q^2} \frac{1}{1-\epsilon} \cdot \Delta\Omega_e \, \Delta E' \cdot \mathcal{L}_{eN} \sim 0.5 \cdot 10^{-5} \cdot \mathcal{L}_{eN} \; = \; 5.5 \cdot 10^{32} \text{ cm}^{-2}\text{s}^{-1},$$

where $E'$ and $\Delta E_e$ are defined by the HRS-right momentum and its range. This leads to the production rate

$$\nu^{\Theta^+}_{e,e' K^- p} = \mathcal{L}_{\gamma^* n} \cdot \sigma^{\Theta^+}_{\gamma n} \cdot f^{HRS}_{\gamma^*, K^-} \cdot f^{decay}_{K^-} \cdot P_{150} \cdot \frac{\Delta\Omega}{4\pi} \; = \; 37 \text{ events per day},$$

where $\mathcal{L}_{\gamma^* n}$ is the virtual photon-neutron luminosity of $5.5 \cdot 10^{32}$ cm$^{-2}$s$^{-1}$; $\sigma^{\Theta^+}_{\gamma n}$ is the cross section of 50 nb; $f^{HRS}_{\gamma^*, K^-}$ is the fraction of $K^-$ associated with $\Theta^+$ production within HRS angular and momentum acceptances, found from MC simulation to be 0.049; $f^{decay}_{K^-} = 0.33$ is the survival probability of a $K^-$ after a 25 meter path in the HRS; $P_{150} = 0.14$ is the probability for a proton in the deuteron to have momentum above 150 MeV/$c$; and $\Delta\Omega$=86 msr is the BigBite solid angle.

#### 5.2.3 Trigger rate and event analysis

The trigger will use a coincidence between two HRSs. The on-line rejection factor of the electrons in HRS-left is 1000 based on the combination the shower detector and the aerogel Čerenkov counter. On-line rejection of hadrons in HRS-right is at least $10^3$ based on the use of a gas Čerenkov counter and a shower counter. A luminosity of $1.1 \cdot 10^{38}$ cm$^{-2}$s$^{-1}$ and 50 ns coincidence time window leads to comfortable coincidence rate of 100 Hz mostly between pions and electrons. The on-line use of the aerogel Čerenkov counter in HRS-left will reject most of pions also. Off-line analysis of the ToF allows us to cut accidental rate by a factor of 25, to a level when both particles are produced in the same beam bunch. Analysis of the event vertex (HRS-left vs HRS-right) allows us to cut the accidental rate by an additional factor of 10 to the level of 0.001 Hz. For real coincidence of the electron and $\pi^-$ two last rejection factors are not applicable, however difference in ToF between kaons and pions is about 1.0 ns which will provide separation by a factor of 20. The real coincidence rate of the electron and $K^-$ is about 0.08 Hz.

The BigBite rate includes a 6.8 MHz soft proton rate and a 14 MHz rate of the pions and electrons. The time window of 42 ns is need for coincidence with HRSs because of the spread of the ToF for our interval of proton momenta. In this first step of the analysis there is an accidental proton in 28% of the $eK^-$ events. On the second step we will use wire chamber. The wire chamber rate will be defined mainly by protons due to the reduced HV setting. The 200 ns time window of the back plane wire chamber and large amplitude pulse in the scintillator will allow us to identify proton track in the back wire chamber plane and the scintillator. The correlation between HRS's event vertex position, position of the proton hit in the back plane and position of the proton trajectory in the front plane allow us identify the right track in the front wire chamber and cut the probability of accidental proton by a factor of 10-15. On this third step we will calculate the proton momentum. The correlation between time-off-flight and reconstructed momentum allow the selection of the reduced time interval of 4-5 ns which lead to cut of accidental hit by a factor of 8-10. After cuts the probability of accidental proton is about 0.23% or the rate of accidental events of 0.00075 Hz, which distributed over 100+ MeV range in the missing mass spectra.

## 5.3 The search for $\Theta^+$ partners (M3)

In this measurement we propose to study reactions H$(e, e'K^-)$X and H$(e, e'K^+)$X. The goal is to find the $\Theta^{++}$ partner and the $\Sigma^\circ_{\overline{10}}$ partner of the $\Theta^+$ state or put very strong limit on its photo-production cross section. The physics motivation for this proposed search was discussed in the Sec. 1. The basic idea - **a tag on high momentum** $K$, as well as, the rate analysis are very similar to the one discussed above.

### 5.3.1 The kinematics

An electron beam with a current of 100 $\mu$A at an energy of 6 GeV will be used. The density of gas will be adjusted to obtain the $\mathcal{L}_{eN}$ of $1 \cdot 10^{38}$ cm$^{-2}$s$^{-1}$. The negative (or positive) kaon will be detected in the magnetic spectrometer HRS-left at a central angle 6° with a septum magnet. The scattered electron will be detected in the magnetic spectrometer HRS-right at central angle 6° with the second septum magnet. There will be three settings of the HRS's magnets. The kinematics for them are similar to the one used in previous measurement. The polarity of HRS-left will be positive in the search for the $\Sigma^\circ_{\overline{10}}$ and negative in search for the $\Theta^{++}$. The momentum settings and other parameters are shown in the Tab. 13.

| run | momentum HRS-left [GeV/$c$] | momentum HRS-right [ GeV/$c$] | mass range [MeV] |
|---|---|---|---|
| $\Theta^{++}$ | -3.0 | -2.1 | 1450-1620 |
| $\Sigma^\circ_{\overline{10}}$ #1 | +3.0 | -1.9 | 1560-1720 |
| $\Sigma^\circ_{\overline{10}}$ #2 | +3.0 | -1.6 | 1700-1860 |

Table 13: The parameters of data taking in the third measurement.

### 5.3.2 The events rate

The estimation of the production rate is quite similar to the shown above for the second measurement. Assuming 0.5 nb production cross section the rate of the $\Theta^{++}$ production is

$$\nu^{\Theta^{++}}_{e,e'K^+} = \mathcal{L}_{\gamma^* p} \cdot \sigma^{\Theta^{++}}_{\gamma n} \cdot f^{HRS}_{\gamma^*, K^-} \cdot f^{decay}_{K^-} \; = \; 700 \text{ events per day},$$

where $\mathcal{L}_{\gamma^* p}$ is the virtual photon-proton luminosity of $1 \cdot 10^{33}$ cm$^{-2}$s$^{-1}$; $\sigma^{\Theta^{++}}_{\gamma n}$ is the cross section of 0.5 nb; $f^{HRS}_{\gamma^*, K^-}$ is the fraction of $K^-$ associated with the $\Theta^{++}$ production within HRS angular and momentum acceptances, found from MC simulation to be 0.049; $f^{decay}_{K^-}$ =

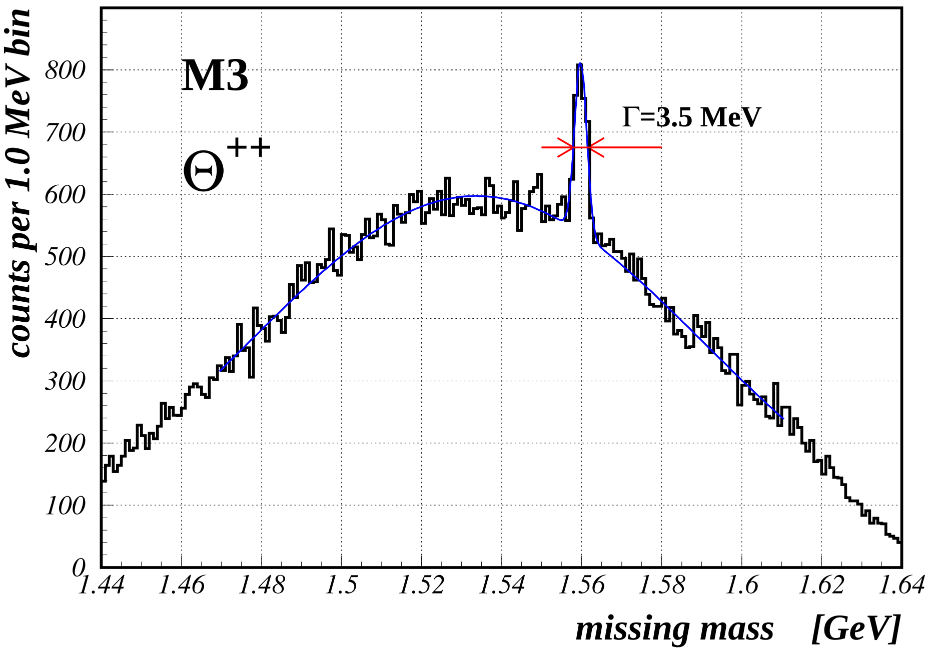


Figure 27: The missing mass spectra expected in the third measurement after 30 hours of data taking, if photo-production cross section of the resonance is 0.5 nb. The peak corresponds to an instrumental resolution (FWHM) = 1.75 MeV and the resonance width (FWHM) = 3 MeV.

0.33 is the survival probability of a $K^-$ after a 25 meter path in the HRS. The simulated missing mass spectra is shown in Fig. 27 for the cross section of the resonance of 0.5 nb with assumed mass of 1560 MeV in 30 hours of data taking. The instrumental resolution of the missing mass in the M3 measurement (FWHM) is about 1.75 MeV. The width of the resonance 3 MeV leads to combined width of the peak of 3.5 MeV. In 45 hours of data taking we can collect about 1300 events in the resonance peak. Non-resonance background under the peak will have about 3400 events. The M3 measurement can easily put an upper limit (two sigma) on the production cross section at the level of 0.05 nb, which is 1/1000 of the $\Theta^+$ state estimated photo-production cross section.

# 6 Expected results and beam time request

## 6.1 Parameters of the $\Theta^+$ state

The analysis presented above was performed for the $\Theta^+$ total photo production cross section of 50 nb (at 4 GeV photon energy), however presently available information doesn't exclude much smaller cross section of 5 nb. The important results on the width and the mass will be obtained with good accuracy even for 5 nb value of the cross section. In the case of larger cross section and statistics additional very interesting results on the $\Theta^+$ quantum numbers will be produced. Two measurements M1 and M2 are providing a very important complementarity, which insure obtaining reliable physics information on the $\Theta^+$ state.

### 6.1.1 The width of the $\Theta^+$

For the width $\Gamma_{res} = 3$ **MeV the experimental result will be** $3.0 \pm 1.0(syst)$ **MeV**. If the production cross section is only 5 nb, then in the invariant mass approach, which provide cleaner event sample, the result will be $3.0 \pm 0.5(stat) \pm 1.0(syst)$ MeV. The expected distributions (for 50 nb cross section) are shown in Figs. 19 and 23.

### 6.1.2 The mass of the $\Theta^+$

In the missing mass approach the absolute value of the $\Theta^+$ mass is defined by knowledge of the beam energy and spectrometers calibration. An accuracy of the absolute calibration of the beam energy of 1.2 MeV for 6 GeV, which was obtained in Hall A [42]; the knowledge of an angle for the central trajectories in HRSs of 1 mr; and an absolute calibration of the HRS momenta on the level of 1 MeV/$c$ lead to an estimate of achievable accuracy for **the value of the $\Theta^+$ mass about 1.3 MeV**.

### 6.1.3 The other results

The differential photo-production cross section $d\sigma/dt$ will be found for the $t - t_\circ$ interval between -0.1 and -0.2 (GeV/$c$)$^2$ in M1 measurement and between 0.0 and -0.1 (GeV/$c$)$^2$ im M2 measurement. The angular distribution of decay products will allow us to find or constrain the spin of the $\Theta^+$ as illustrated in Fig. 20. The $\Sigma$ photon asymmetry will be measured with an accuracy $\approx 0.05$, which may be sufficient for distinction between negative and positive parity of the $\Theta^+$.

## 6.2 Search for partners of the $\Theta^+$ state

The experiment will find the $\Theta^{++}$ or put an upper limit on the photo-production cross section of $\Theta^{++}$ at the level of 0.05 nb in the mass interval 1450-1620 MeV. Similar result for the $\Sigma^\circ_{\overline{10}}$ will be obtained in the mass interval 1560 - 1860 MeV.

### 6.3 Beam time request

The purpose of this experiment is to measure the parameters of the the $\Theta^+$ state and a search for its partners. The experiment will be performed at two beam energies 4.5 and 6.0 GeV, with currents up to 110 $\mu$A. Table 14 summarizes the beam time for data taking. We plan to do measurements in order M3, M2, M1. The M3 measurement is the most simple to prepare and it will allow us to tune kinematical conditions for the two triple coincidence measurements. The M2 measurement requires of the BigBite for detection of the soft proton. Most of new equipment in this run is under construction for the ChPT experiment E01-014 [20]. The M1 measurement needs more complicated installation and the detectors of the GEN experiment E02-013 [21]. If the full energy of 6.0 GeV will be not available, a slight change of the spectrometers momenta settings will be done.

| kin. M# | type of measurement | current [$\mu$A] | energy [GeV] | time [hr] |
|---|---|---|---|---|
| | HRS and BigBite calibration | 10 | 2.0 | 12 |
| | beam energy measurement | 1 | 6.0 | 4 |
| M3 | partners search | 100 | 6.0 | 140 |
| M2 | $\Theta^+$ via missing mass | 110 | 6.0 | 480 |
| M1 | $\Theta^+$ via invariant mass | 20 | 4.5 | 480 |
| total | | | | 1116 |

Table 14: The time allocation assuming 100% efficiency.

In total we request 47 days of beam-time to perform the proposed measurements.

# 7 Conclusions

We request 1116 hours of beam-time to measure the electro-production of $\Theta^+$ resonance in two reactions and to conduct a search of the possible $\Theta^{++}$ and $\Sigma^{\circ}_{\overline{10}}$ partners. Measurement of the width with instrumental resolution (rms) of 1.3 MeV will reveal the state's width and enhance understanding of the nature of this exotic state. The value of the mass will be established with an accuracy of 1.3 MeV. Furthermore, the proposed experiment will collect a sample of about 1800 $\Theta^+$ events (for assumed 50 nb production cross section) and investigate the resonance properties. We propose an experiment, which can establish the nature of the resonance. Status of the equipment needed in the proposed measurements should permit the experiment to be realized in a time scale of one to two years. Additional resources may allow a reduction in preparation time.

## References


[1] D. Diakonov, V. Petrov, and M. Polyakov, *Z. Phys. A.* **359**, 305 (1997).

[2] F. Csikor *et al.*, hep-lat/0309090.

[3] T. Nakano *et al.*, [LEPS Collaboration], *Phys. Rev. Lett.* **91**, 012002 (2003).

[4] V.V. Barmin *et al.*, [DIANA Collaboration] Phys. Atom. Nuclei **66**, 1715 (2003).

[5] S. Stepanyan *et al.*, [CLAS Collaboration], to be published in *Phys. Rev. Lett.* , hep-ex/0307018.

[6] V. Koubarovsky and S. Stepanyan, [CLAS Collaboration], in: *Proceedings of "Conference on the Intersections of Particle and Nuclear Physics (CIPANP2003), New York, NY, USA, May 19-24, 2003"*; hep-ex/0307088.

[7] J. Barth *et al.*, [SAPHIR Collaboration], *Phys. Lett.* **B572**, 127 (2003).

[8] A. E. Asratyan *et al.*, to be published in Phys. Atom. Nuclei; hep-ex/0309042.

[9] A. Airapetian and M. Amarian [HERMES Collaboration], http://www-hermes.desy.de/notes/pub/trans-public-subject.html #EXOTICS

[10] R. Jaffe and F. Wilczek, hep-ph/0307341.

[11] M. Karliner and H. J. Lipkin, hep-ph/0307243.

[12] E. Shuryak and I. Zahed, hep-ph/0310270.

[13] S. Capstick *et al.*, *Phys. Lett.* **B570**, 185 (2003).

[14] F. Stancu and D. O. Riska, *Phys. Lett.* **B575**, 242 (2003).

[15] N. Auerbach and V. Zelevinsky, hep-ph/0310029.

[16] S. Nussinov, hep-ph/0307357.

[17] R. A. Arndt, I. I. Strakovsky, and R. L. Workman, *Phys. Rev. C* **68** , 042201 (2003).

[18] J. Haidenbauer and G. Krein, hep-ph/0309243, to be published in *Phys. Rev. C* .

[19] C. Alt *et al.*, [NA49], submitted to *Phys. Rev. Lett.* , hep-ex/0310014.

[20] J. Annand, D. Higinbotham, R. Lindgren, V. Nelyubin, B. Norum, spokespersons, JLab experiment E01014.

[21] G. Cates, B. Reitz, K. McCormick, and B. Wojtsekhowski, spokespersons, JLab experiment E02-013.

[22] Haiyan Gao and Bo-Qiang Ma, *Mod. Phys. Lett. A* **14**, 2313 (1999) [hep-ph/0305294].

[23] B. Wojtsekhowski *et al.*, in Hall A annual report, p.31 (2002).

[24] F. Garribaldi, private communication (2003).

[25] D. J. J. de Lange *et al.*, *Nucl. Instr. Meth.* A **406**, 182 (1998); D. J. J. de Lange *et al.*, *Nucl. Instr. Meth.* A **412**, 254 (1998).

[26] L. Tang *et al.*, HKS report for JLab readiness review, (2003).

[27] P. V. Degtyarenko, "Applications of the Photo-nuclear Fragmentation Model to Radiation Protection Problems", Proceedings of the Second Specialist's Meeting on Shielding Aspects of Accelerators, Targets and Irradiation Facilities (SATIF2), 12-13 October 1995, CERN, Geneva, Switzerland, p. 67; P. V. Degtyarenko, M. V. Kossov, and H-P. Wellisch, Chiral Invariant Phase Space Event Generator, I. Nucleon-antinucleon annihilation at rest, Eur. Phys. J. A **8**, p. 217 (2000).

[28] B. Wojtsekhowski, P. Degtyarenko, R. Lindgren, "A New Tool For Correlation Studies in Hall A at JLAB, JLab-TN-01-047", report on 5th Workshop on Electromagnetically Induced Two-Hadron Emission, Lund, Sweden, (2001).

[29] P. V. Degtyarenko, GEN collaboration meeting, 05/24/2003, http://hallaweb.jlab.org/experiment/E02-013/collabmeetings.html.

[30] P. V. Degtyarenko, GEN collaboration meeting, 10/24/2003, http://hallaweb.jlab.org/experiment/E02-013/collabmeetings.html.

[31] H. Burfeint *et al.*, *Phys. Lett.* **43B**, 345 (1973).

[32] H. Burfeint *et al.*, *Nucl. Phys.* **B74**, 189 (1974).

[33] A. M. Boyarski *et al.*, *Phys. Rev. D* **14**, 1733 (1976).

[34] R. Feynmann, *Phys. Rev. Lett.* **23**, 1415 (1969).

[35] J. Benecke *et al.*, *Phys. Rep.* **188**, 2159 (1969).

[36] V. M. Budnev *et al.*, *Phys. Rep.* **15**, 181 (1974).

[37] J. Adam Jr. *et al.*, *Phys. Rev. C* **66** 044003 (2002).

[38] V. Kubarovsky [CLAS collaboration], report on the Pentaquark workshop, JLab 11/6-8, 2003.

[39] W. Liu and C. M. Ko, nucl-th/0309023.

[40] K. Nakayama and K. Tsushima, hep-ph/0311112.

[41] M. Guidal, M. V. Polyakov, and M. Vanderhaeghen, report on the Pentaquark workshop, JLab 11/6-8, 2003.

[42] J. Alcorn *et al.*, accepted for publication in *Nucl. Instr. Meth.* A.